

CONFIDENTIAL

FP7-ICT Future Networks
SPECIFIC TARGETTED RESEARCH PROJECT
Project Deliverable

PHYDYAS Doc. Number	PHYDYAS_ 003
Project Number	ICT - 211887
Project Acronym+Title	PHYDYAS – PHYsical layer for DYnamic AccesS and cognitive radio
Deliverable Nature	Report
Deliverable Number	D3.1
Contractual Delivery Date	July 1 st , 2008
Actual Delivery Date	July 28, 2008
Title of Deliverable	Equalization and demodulation in the receiver (single antenna)
Contributing Workpackage	WP3
Project starting date; Duration	01/01/2008; 30 months
Dissemination Level	CO
Author(s)	Jérôme Louveaux (UCL-WP3 leader), Leonardo Baltar, Dirk Waldhauser (TUM), Markku Renfors (TUT), Mario Tanda (UNINA), Carlos Bader (CTTC), Eleftherios Kofidis (RA-CTI)

Abstract: In filter bank based multicarrier (FBMC) systems, it is appropriate to carry out the equalization function in the frequency domain, at the sub-channel level. The process starts with channel estimation, using pilot signals, and the scheme has to take into account the specificity of OQAM modulation. Different types of equalizer are presented and their performances are evaluated. The compensation of residual synchronization errors is investigated. Then, considering the WiMAX scenario, a detailed comparison of the equalizer structures is performed, in order to select the most efficient implementation for the demonstrator.

The next step is the delivery of the corresponding software to WP9 for simulation and evaluation.

Contents

1 INTRODUCTION: FILTER BANK BASED MULTICARRIER (FBMC) TRANSMISSION PRINCIPLE	7
1.1 The filter bank technique	7
1.2 Description of the reference filter bank	9
1.2.1 Choice of filter bank structure	9
1.2.2 Frequency-sampling based design of prototype filter	10
1.2.3 Polyphase filter bank structure	11
1.2.4 Model for ideal FBMC transmission link	14
2 GENERAL SCOPE OF WP3: EQUALIZATION	15
3 CHANNEL ESTIMATION	18
3.1 Auxiliary pilot scheme	18
3.2 Application of auxiliary pilot scheme to WiMAX pilot structures	22
3.3 Preamble-Based Schemes	24
3.3.1 Estimation Using the Pairs of Pilots (POP) Method	25
3.3.2 Estimation Using the Interference Approximation Method (IAM)	26
3.3.3 Simulation Results with Preamble-Aided Channel Estimation	27
3.3.4 Adaptation to the DL PUSC communication mode	29
3.4 Interpolation of pilot-based channel estimates	32
3.4.1 Two dimensional estimation	32
3.4.2 Separable filters	33
4 EQUALIZER STRUCTURES	34
4.1 Frequency sampling approach	34
4.1.1 Approach 1	34
4.1.2 Approach 2	36
4.2 Multiple taps equalizers	40
4.2.1 Fractionally spaced MMSE Per-Subcarrier Equalizer	40
4.2.2 Simplified MMSE equalizer:	43
4.3 Multiple band MMSE equalizer:	44
4.4 Fractionally Spaced Adaptive (LMS) Per-Subcarrier Equalization	48
4.5 CFO compensation	50
4.6 Timing compensation	52

4.6.1 Performance evaluation of frequency-domain timing offset compensation using subcarrier equalizers 52

4.6.2 Interference minimization approach to timing offset compensation 53

4.7 Multi-user uplink aspects 54

5 COMPARISON RESULTS 55

6 CONCLUSIONS AND FUTURE WORKS 57

7 REFERENCES 58

Notations

$\angle\{x\}$	the argument of a complex number x in $[0, 2\pi)$,
$\text{Re}\{\cdot\}$	real part
$\text{Im}\{\cdot\}$	imaginary part
$(\cdot)^*$	complex conjugation
$ \cdot $	absolute value
M	overall number of subcarriers, FFT size
M_u^i	number of used subcarriers of the i th user (in single-user case, index i is dropped)
M_u^i	set of used subcarriers of the i th user
M_v	number of virtual (unused) subcarriers
K	overlapping factor in prototype filter design
α	roll-off factor in prototype filter design
L	prototype filter length
T_s	sampling interval (at SFB output and AFB input)
f_s	sampling rate (at SFB output and AFB input)
T	OQAM symbol duration; $T=MT_s$
Δf	subcarrier spacing, $\Delta f=1/T=f_s/M$
k	subcarrier index ($k=0, \dots, M-1$; $k=0$ corresponds to center subcarrier)
n	time index at subcarrier rate
m	time index at SFB output/AFB input
i	user index in multiuser cases
U	number of users
$v^R(n)$	real part of (arbitrary) complex sequence $v(n)$
$v^I(n)$	imaginary part of (arbitrary) complex sequence $v(n)$
$p(t)$	prototype filter impulse response, continuous-time model
$p(m)$	prototype filter impulse response, discrete-time ⁽¹⁾ $p(m) = \sqrt{T_s} p(mT_s)$
$P(z)$	prototype filter transfer function
$f_k(m)$	analysis filter impulse response for subchannel k
$F_k(z)$	analysis filter transfer function for subchannel k
$G_k(z)$	synthesis filter transfer function for subchannel k
$g_k(m)$	synthesis filter impulse response for subchannel k $g_k(m) = p(m) e^{j \frac{2\pi}{M} k \left(m - \frac{L-1}{2} \right)}$
$p_{k,n}(m)$	SFB impulse response for real symbol $d_{k,n}$ (see also definition of $s(m)$) $p_{k,n}(m) = \theta_{k,n} g_k(m - nM/2)$ $= \theta_{k,n} \beta_{k,n} p(m - nM/2) e^{j \frac{2\pi}{M} km}$
$\theta_{k,n}$	phase mapping between real data sequence and complex samples at the SFB input
In general,	
$\theta_{k,n} = \begin{cases} \pm 1 & \text{for } k+n \text{ even} \\ \pm j & \text{for } k+n \text{ odd} \end{cases}$	

The recommended choice (following Siohan's papers) is⁽²⁾:

$$\theta_{k,n} = j^{k+n}$$

$$\beta_{k,n} = e^{j2\pi k \left(-\frac{n}{2} - \frac{L-1}{2M} \right)}$$

$d_{k,n}$ transmitted sequence of the i th user (data & pilots) (real)

$x_{k,n}$ observed ideal (without channel) complex sample sequence at AFB output

$$x_{k,n} = \begin{cases} d_{k,n} + ju_{k,n} & \text{for } k+n \text{ even} \\ u_{k,n} + jd_{k,n} & \text{for } k+n \text{ odd} \end{cases}$$

Here $u_{k,n}$ is the un-interesting part of the received complex samples.

$y_{k,n}$ observed channel-distorted complex sample sequence at AFB output

$\tilde{d}_{k,n}$ subcarrier sequence after equalization (real)

$\hat{d}_{k,n}$ detected sequence (real)

$s(m)$ transmitted sequence at SFB output, single user case

$$\begin{aligned} s(m) &= \sum_{k \in \mathbb{M}_u} \sum_{n=-\infty}^{\infty} d_{k,n} \theta_{k,n} g_k(m - nM/2) \\ &= \sum_{k \in \mathbb{M}_u} \sum_{n=-\infty}^{\infty} d_{k,n} \theta_{k,n} p(m - nM/2) e^{j\frac{2\pi}{M}k \left(m - n\frac{M}{2} - \frac{L-1}{2} \right)} \\ &= \sum_{k \in \mathbb{M}_u} \sum_{n=-\infty}^{\infty} d_{k,n} \theta_{k,n} (-1)^{kn} p(m - nM/2) e^{j\frac{2\pi}{M}k \left(m - \frac{L-1}{2} \right)} \\ &= \sum_{k \in \mathbb{M}_u} \sum_{n=-\infty}^{\infty} d_{k,n} \theta_{k,n} \beta_{k,n} p(m - nM/2) e^{j\frac{2\pi}{M}km} \\ &= \sum_{k \in \mathbb{M}_u} \sum_{n=-\infty}^{\infty} d_{k,n} p_{k,n}(m) \end{aligned}$$

$s_i(m)$ transmitted sequence at SFB output in the uplink multiuser FBMC system, e.g.,

$$s_i(m) = \sum_{k \in \mathbb{M}_u^i} \sum_{n=-\infty}^{\infty} d_{k,n} p_{k,n}(m)$$

$s(t)$ transmitted continuous-time signal ($s_i(t)$ correspondingly for user i in multiuser case)

$$s(t) = \sum_{k \in \mathbb{M}_u} \sum_{n=-\infty}^{\infty} d_{k,n} \theta_{k,n} (-1)^{kn} p\left(t - n\frac{T}{2}\right) e^{j2\pi k \left(\Delta f t - \frac{L-1}{2M} \right)}$$

$r(t)$ received continuous-time signal in the uplink multiuser FBMC system

$$r(t) = \sum_{i=1}^U e^{j2\pi(\frac{\varepsilon_i}{T}t)} h_i(t, \tau) * s_i(t) + n(t) \quad \text{general case}$$

$$r(t) = \sum_{i=1}^U e^{j2\pi(\frac{\varepsilon_i}{T}t)} \sum_{p=0}^{P_i-1} c_{i,p} s_i(t - \tau_{i,p}) + n(t) \quad \text{discrete multipath case}$$

$$r(t) = \sum_{i=1}^U e^{j2\pi(\frac{\varepsilon_i}{T}t)} c_i s_i(t - \tau_i) + n(t) \quad \text{AWGN case}$$

$$= \sum_{i=1}^U e^{j2\pi(\frac{\varepsilon_i}{T}t + \phi_i)} |c_i| s_i(t - \tau_i) + n(t)$$

ε_i carrier frequency offset of the i th user, normalized to subcarrier spacing

ϕ_i carrier phase offset (radians) of the i th user in the AWGN model

$h_i(t, \tau)$ time-variant channel impulse response of i th user

P_i number of paths in the multipath channel model of user i

$c_{i,p}$ complex gain of the p th path of the channel of user i

$\tau_{i,p}$ delay of the p th path of the channel of user i

τ_i timing offset of the i th user in the AWGN model

$n(t)$ complex envelope of white (Gaussian) noise whose real and imaginary parts are statistically independent and have a power spectral density level of N_0

σ_n^2 channel noise variance

N_0 one-sided noise power spectral density of white channel noise

$r(m)$ received complex sequence at AFB input

$n(m)$ channel noise

$h_i(m)$ discrete-time channel impulse response for user i in block-fading model

$H_i(e^{j\omega})$ channel frequency response for user i

H_k channel response of subcarrier k (assuming flat-fading and time invariant/block-fading case)

$H_{k,n}$ channel response for subcarrier k and symbol n (assuming flat-fading and time variant case)

$H_{k,n}^{p,q}$ channel response for subcarrier k and symbol n from TX antenna p to RX antenna q

$w_k(n)$ subcarrier-wise channel equalizer impulse response for subchannel k

Notes:

(1) This assumes causal continuous-time prototype filter impulse response, which is different from Siohan's continuous-time model.

(2) The choice of $\theta_{k,n}$, i.e., the signs in mapping real data sequence to complex samples at the SFB input is an internal choice of the filter bank module (i.e., the definition of $x_{k,n}$ above can be assumed to be valid in any case). However, it has an effect on the signal models at the SFB output and for the complex sequences at the AFB output. In the receiver side, $\beta_{k,n}^*$ is implemented before the subband processing, and $\theta_{k,n}^*$ after it. With this choice, all the subchannels are centered at DC at the subchannel processing stage.

1 Introduction: Filter bank based multicarrier (FBMC) transmission principle

Note: In order to have a self-contained deliverable, the description of the FBMC transmission scheme has been rewritten here. This section is a copy from deliverable D2.1.

Multicarrier transmission techniques based on digital filter banks were developed in the seventies to perform the conversion between PCM (Pulse Code Modulation) and FDM (Frequency Division Multiplexing) systems. In the nineties, OFDM (Orthogonal Frequency Division Multiplexing) was preferred because it was considered simpler in concept, less complex and it had minimum latency. Now, radio communications are moving in directions that make the objections to the filter bank approach unfounded and, in fact, make filter banks particularly attractive. First, in order to achieve quality of service (QoS) and high throughput, radio transmission is resorting to multi-antenna terminals (MIMO), which is a considerable increase in complexity. Moreover, when combined with multicarrier transmission, the MIMO principle requires high resolution spectrum analysis to accurately estimate the channel matrix. Second, communications are migrating to all-IP networks, which implies packet transmission and, therefore, minimum latency at the physical (PHY) layer is no longer crucial and the actual constraints are put on the upper layers. Scalability is a function that is being introduced and it is easily implemented with filter banks because of the independence of sub-channels. In addition, the new concepts of DASM (Dynamic Access Spectrum Management) and cognitive radio require high resolution spectral analysis, a functionality in which filter banks superior over the discrete Fourier transform of OFDM.

1.1 The filter bank technique

The principle of transmission based on filter banks is shown in Figure 1-1 [1][2]. The transmitter contains a synthesis filter bank (SFB) and the receiver contains an analysis filter bank (AFB). In the structure of the figure, the FFT (Fast Fourier Transform) is present as in OFDM. It is augmented, to complete a filter bank, by the PPN (Polyphase Network) which consists of a set of digital filters, whose coefficients, globally, form the impulse response of the so-called prototype low-pass filter.

The essential difference between FBMC and OFDM resides in the frequency selectivity. This is illustrated in Figure 1-2, which shows the frequency responses, around a particular sub-carrier, in both cases. OFDM exhibits large ripples in the frequency domain, which imposes the orthogonality constraint between all the sub-carriers. On the contrary, the filter bank frequency response has a negligible amplitude beyond the center frequency of the adjacent sub-carriers. In fact, the filter bank divides the transmission channel of the system into a set of sub-channels and any sub-channel overlaps with its immediate neighbors only. Then, in order to make two groups of contiguous sub-channels independent, it is sufficient to leave a single empty subchannel between them.

The difference in frequency responses between FBMC and OFDM shown in Figure 1-2 has a considerable impact on the performance of wireless systems and their operational flexibility. The FBMC approach has the following features:

- no guard time, or cyclic prefix, is needed,
 - full capacity of the transmission bandwidth is achieved using OQAM (Offset Quadrature Amplitude Modulation),
 - frequency mask constraints for the transmitted signals are easily satisfied,
-

- sub-channels can be grouped into independent blocks, which is crucial for scalability and dynamic access, for example,
- with the absence of leakage in the frequency domain, high resolution spectral analysis is achieved,
- the same device can be used in cognitive radio for spectrum sensing and reception, even simultaneously, which guaranties perfect coherence between the two functions.

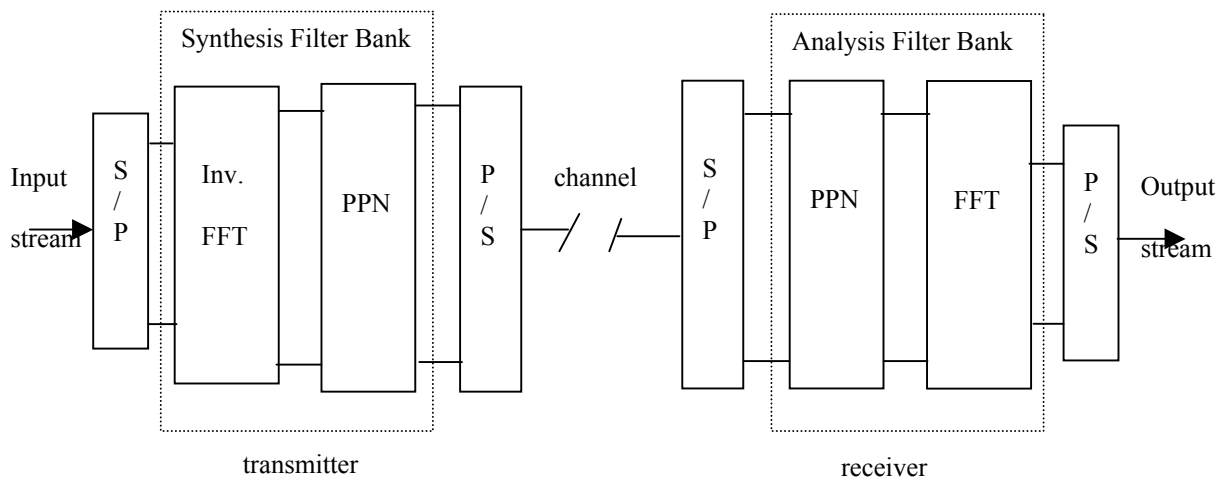


Figure 1-1. Filter Bank-based Multi-Carrier (FBMC) system.

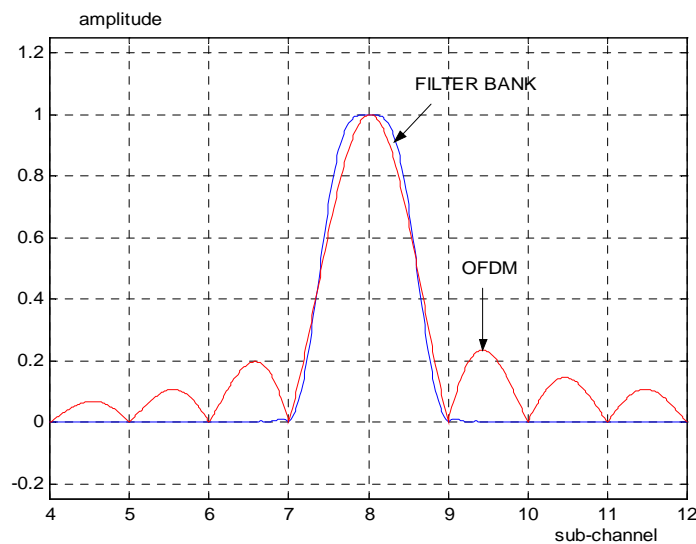


Figure 1-2. Comparison of frequency responses of FBMC and OFDM.

1.2 Description of the reference filter bank

The analysis and synthesis filter banks are naturally the key components in the PHYDYAS project. We start this chapter with a brief discussion concerning general issues related to the choice and characteristics of the filter banks to be used. Then the design method for PHYDYAS reference filter, to be used during the initial phase of the project, is described. In Section 1.2.3, a more detailed description of the polyphase filter banks structures and related signal models are presented, and in Section 1.2.4 the characteristics of an ideal FBMC transmission link using the reference filter bank are discussed.

In PHYDYAS, the Work Package 5 is focusing on the further optimization of the filter banks for use during the later phases of the project. The work on filter bank design aspects in the FBMC context will be reported in Deliverable D5.1.

1.2.1 Choice of filter bank structure

A basic constraint of data transmission is that the channel must satisfy the Nyquist criterion, to avoid intersymbol interference. If the symbol period is T_{symp} and the symbol rate is $f_{\text{symp}}=1/T_{\text{symp}}$, the channel frequency response must be symmetrical about the frequency $f_{\text{symp}}/2$. Accordingly, in FBMC, the prototype filter for the synthesis and analysis filter banks must be half-Nyquist, which means that the square of its frequency response must satisfy the Nyquist criterion.

In this work we consider uniform filter banks, i.e., all the subchannels have the same bandwidth. Efficient uniform filter banks can be implemented using various structures utilizing modulation to create bandpass subchannel filters from a single lowpass prototype filter, basically through frequency-shifting. There are various efficient multirate structures for the needed filter banks, including lapped transforms, lattice structures, and the polyphase structure [3]-[5]. Common to all these structures is that they consist of a filter section, the coefficients of which is determined by the prototype filter design, and a transform section (e.g., discrete Fourier, sine or cosine transforms) implementing the modulation. In combination with the transform blocks, the structures include sampling rate conversion operations, such that the subchannel signals operate at the basic signaling rate, whereas the synthesized wideband signal has a much higher sampling rate.

In a critically sampled filter bank system, the sample rate (counted in terms of real-valued samples in the possible complex (I/Q) signals) of the SFB output and AFB input is equal to the sum of the sample rates of the subchannel signals. In the FBMC application, the use of critically sampled filter banks would be problematic, since the aliasing effects would make it difficult to compensate imperfections of the channel by processing the subchannel signals after the AFB only. Therefore, a factor of two oversampling is commonly applied in the subchannel signals in the AFB. In the considered filter bank models, the useful data symbols are carried alternately by real and imaginary parts of the complex-valued subcarrier sequences (in an alternative scheme, the data is in the real parts only [6]). By using the whole complex samples in subchannel processing in the receiver, effectively 2x oversampling is obtained. At the end of the subchannel processing sections, the needed real/imaginary parts are selected to get a critically sampled sequence for detection.

So-called perfect-reconstruction (PR) filter banks implement the Nyquist criterion exactly and also without introducing any cross-talk between subchannels in the back-to-back connection of SFB and

AFB (so-called transmultiplexer). In wireless communications, the transmission channel introduces inevitably some distortion to the received subchannel signals. Therefore, the PR condition is not essential, and it is sufficient that the cross-talk between subchannels is small enough to be ignored in comparison to the residual interference, e.g., due to imperfect channel equalization. From the filter bank design point of view, this means that the so-called nearly perfect-reconstruction (NPR) designs are sufficient. Since NPR designs are more efficient than PR designs, e.g., in providing higher frequency selectivity with given prototype filter length, NPR designs are the favored choice in PHYDYAS. For NPR filter banks, the polyphase structure is the natural choice, since lapped transforms and lattice structure can be used only in the PR case [3]-[5].

During the first phase of the PHYDYAS project, the work is based on a selected filter bank design known from the literature [2]. This filter bank is based on the polyphase structure and analytical formulas for calculating the filter coefficients for a wide choice of the main parameters:

- The number of subchannels (M) is basically arbitrary, but typically a power of 2 is used in order to be able to use IFFT/FFT as efficient algorithms for the transform blocks.
- Overlapping factor (K) can be selected to be 3 or higher. The basic choice for prototype filter length is $L=KM$, but also $L=KM+1$ or $L=KM-1$ are interesting alternatives.
- The roll-off parameter of this design is essentially $\alpha=1$, which means that the transition bands of a subchannel end at the centers of the adjacent subchannels. This means that only immediately adjacent subchannels are significantly interacting with each other.

1.2.2 Frequency-sampling based design of prototype filter

A simple technique to design the prototype filter is the so-called frequency sampling technique, which is presented with the following parameters

$$L = 2048; M = 512; K = 4.$$

The design starts with the determination of L desired values $H(k/L); 0 \leq k \leq L-1$ in the frequency domain by

$$\begin{aligned} H(0) &= 1 \\ H(1/L) &= 0.971960 \\ H(2/L) &= 1/\sqrt{2} \\ H(3/L) &= \sqrt{1-H^2(1/L)} = 0.235147 \\ H(k/L) &= 0 \quad ; \quad 4 \leq k \leq L-1 \end{aligned} \tag{1}$$

Then, the prototype filter coefficients are obtained by inverse DFT as

$$\begin{aligned} h(m) &= 1 + 2 \sum_{k=1}^{K-1} (-1)^k H(k/L) \cos(2\pi km/L) ; \quad 1 \leq m \leq L-1 \\ h(0) &= 0 \end{aligned} \tag{2}$$

In fact, the condition $h(0) = 0$ determines the desired values $H(1/L)$ and $H(3/L)$. It is useful to make the number of coefficients an odd number, in which case the filter delay can be adjusted to be an integer number of sample periods.

The frequency response obtained is shown in Figure . In this figure, the sub-channel spacing Δf is taken as unity ($\Delta f=1$). It is important to notice that the filter attenuation exceeds 60 dB for the frequency range above 2 sub-channel spacings.

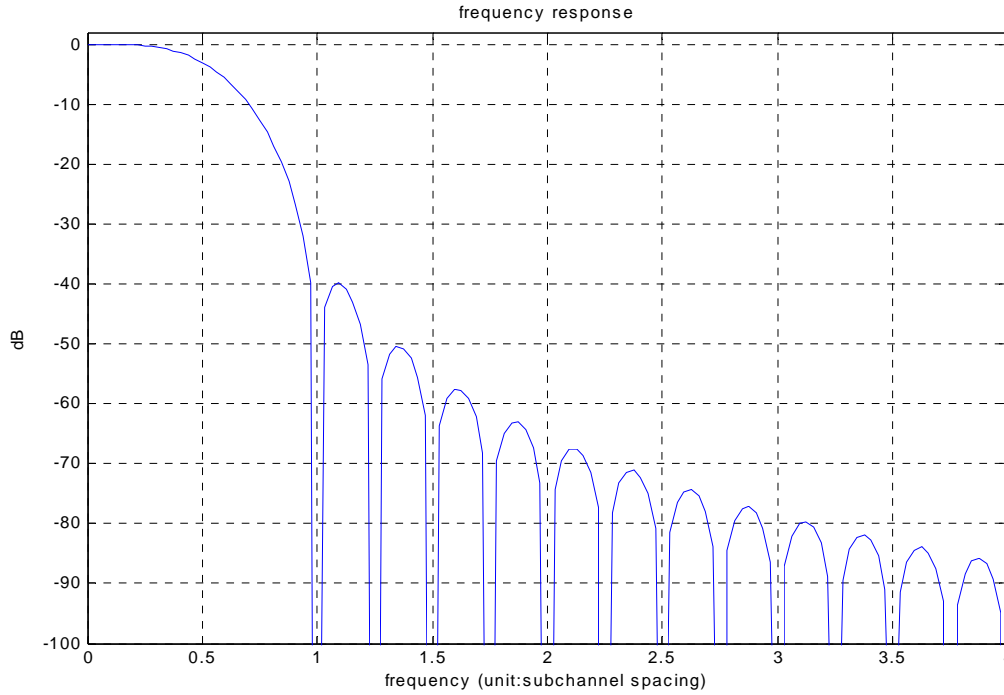


Figure 1-3. Frequency response of the prototype filter.

1.2.3 Polyphase filter bank structure

Figure 1-4 shows the polyphase structures for synthesis and analysis filter banks [1]-[6]. The discrete-time baseband signal at the output of the synthesis bank of an FBMC transmitter based on offset-QAM (OQAM) modulation can be expressed as

$$s(m) = \sum_{k \in \mathbb{M}_t} \sum_{n=-\infty}^{\infty} d_{k,n} \theta_{k,n} g_k(m - nM/2) \quad (3)$$

where

$$\begin{aligned} \theta_{k,n} &= j^{(k+n)} \\ d_{k,n} &= (-1)^{kn} \end{aligned} \quad (4)$$

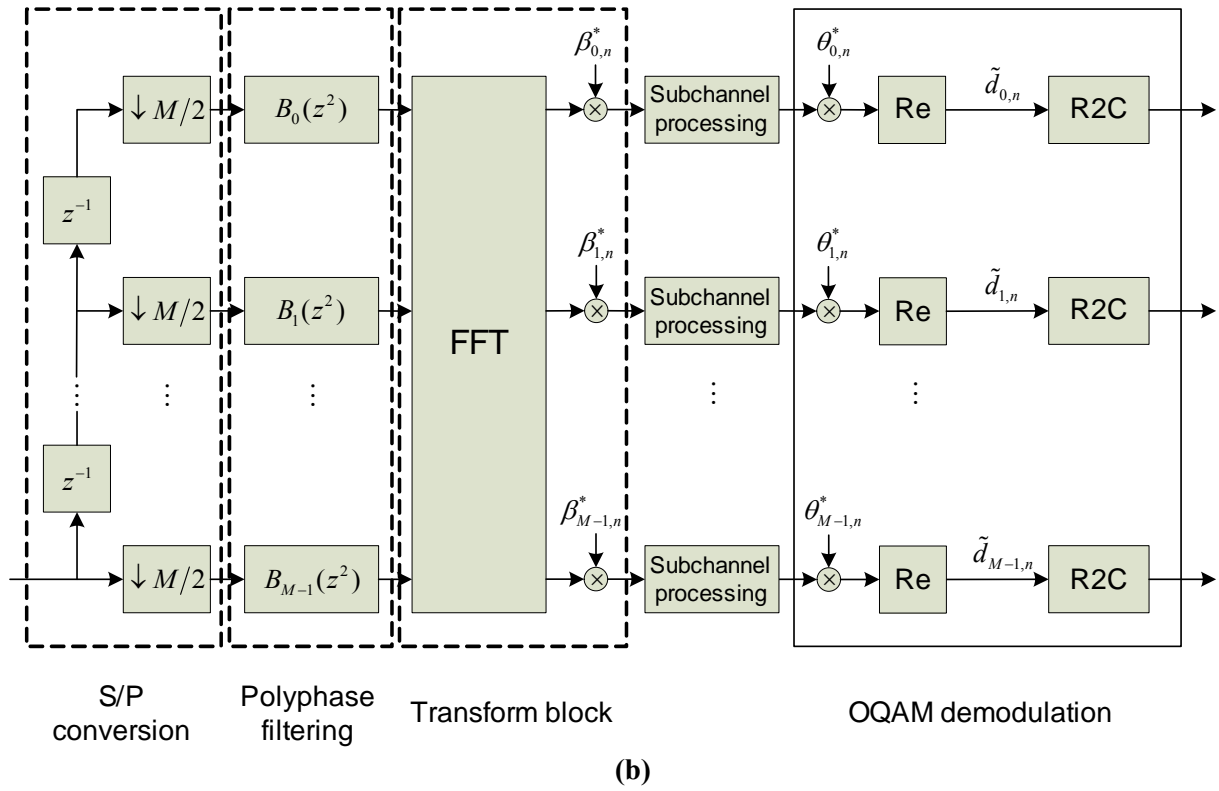
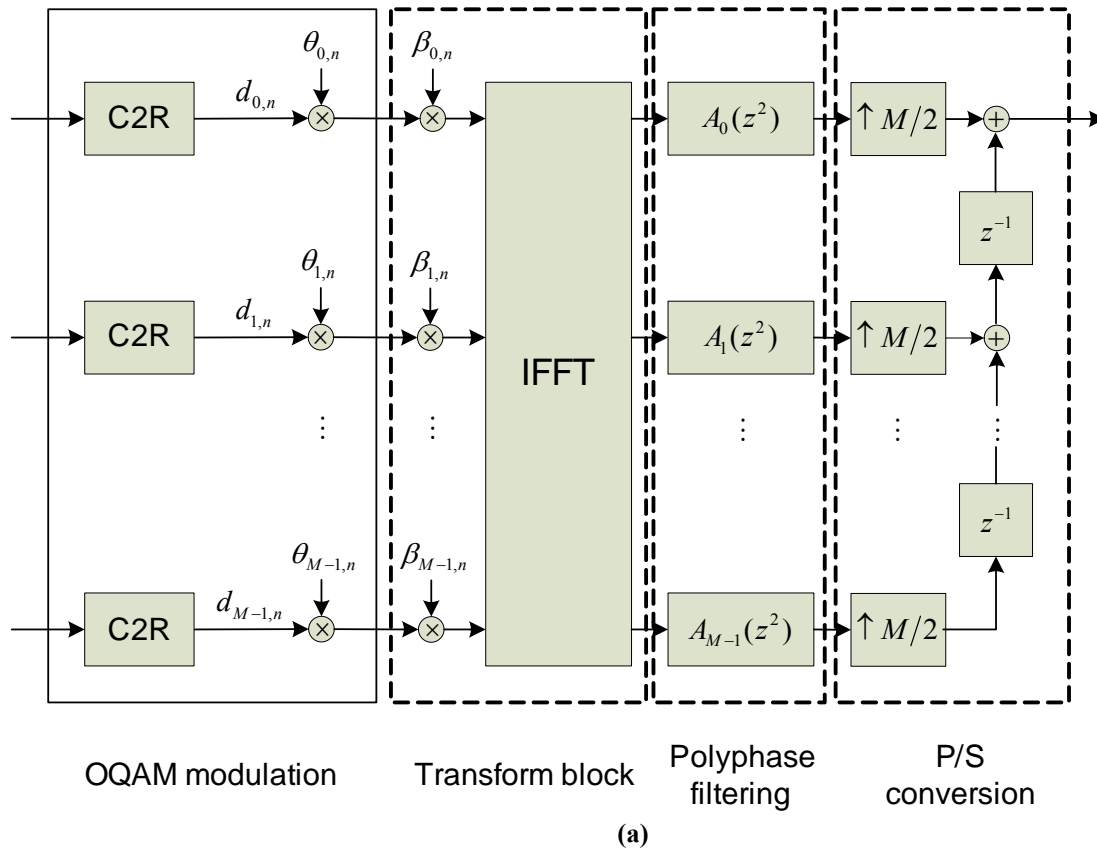


Figure 1-4. Polyphase filter bank structures. (a) Synthesis bank (SFB). (b) Analysis bank (AFB).

Here M is the overall number of subcarriers (=IFFT/FFT size), M_u is the set of active subcarriers, and $d_{k,n}$ denotes the real-valued symbols at the k th subcarrier during the n th symbol interval, modulated at rate $2/T$. The signaling interval T is defined as the inverse of the subcarrier spacing, i.e., $T = 1/\Delta f$. The symbols $d_{k,n}$ and $d_{k,n+1}$ can be interpreted to carry the In-phase and Quadrature (I/Q) components of the complex-valued symbol $c_{k,l}$ (of rate $1/T$) from a QAM-alphabet. It should be noted that the signs of the $\theta_{k,n}$ sequence can be chosen arbitrarily, but the pattern of real and imaginary samples has to follow this definition to maintain (near) orthogonality [1].

In (3), $g_k(m)$ are shift-invariant impulse responses of the SFB channel filters. The signal model can also be written in terms of the prototype filter impulse response, $p(m)$, of length L , as follows:

$$\begin{aligned} s(m) &= \sum_{k \in M_u} \sum_{n=-\infty}^{\infty} d_{k,n} \theta_{k,n} p(m - nM/2) e^{j\frac{2\pi}{M}k\left(m - n\frac{M}{2} - \frac{L-1}{2}\right)} \\ &= \sum_{k \in M_u} \sum_{n=-\infty}^{\infty} d_{k,n} \theta_{k,n} \beta_{k,n} p(m - nM/2) e^{j\frac{2\pi}{M}km} \end{aligned} \quad (5)$$

where

$$\beta_{k,n} = e^{-jkn\pi} \cdot e^{-j\frac{k}{M}(L-1)\pi} = (-1)^{kn} \cdot e^{-j\frac{k}{M}(L-1)\pi} \quad (6)$$

From the latter form of (5), the different parts of the polyphase SFB structure of Figure 1-4(a) can be identified.

We can use also the following short-hand notation for the signal model:

$$s(m) = \sum_{k \in M_u} \sum_{n=-\infty}^{\infty} d_{k,n} p_{k,n}(m) \quad (7)$$

where

$$p_{k,n}(m) = \theta_{k,n} \beta_{k,n} p(m - nM/2) e^{j\frac{2\pi}{M}km}. \quad (8)$$

The synthesized signal burst is therefore a composite of multiple subchannel signals each of which consists of a linear combination of time-shifted (by multiples of $T/2$), frequency-shifted, and overlapping impulse responses of the prototype filter, weighted by the respective symbol values $d_{k,n}$.

The continuous-time model for the transmitted waveform can be written as

$$s(t) = \sum_{k \in M_u} \sum_{n=-\infty}^{\infty} d_{k,n} \theta_{k,n} (-1)^{kn} p\left(t - n\frac{T}{2}\right) e^{j2\pi k\left(\Delta f t - \frac{L-1}{2M}\right)} \quad (9)$$

where $p(t)$ is the continuous-time impulse response corresponding to the prototype filter design.

1.2.4 Model for ideal FBMC transmission link

The transmultiplexer, i.e., the back-to-back connection of an SFB and AFB, is a fairly complicated multirate signal processing structure, and the expression of the AFB output subchannel samples in terms of the SFB subchannel samples and prototype filter impulse response is rather complicated. It is not included here, but we present a simplified model instead. In case of ideal channel, the complex oversampled subchannel signals in AFB can be expressed as

$$x_{k_0, n_0} = \sum_{k \in M_u} \sum_{n=-\infty}^{\infty} d_{k,n} \theta_{k,n} t_{k_0-k, n_0-n} \quad (10)$$

The transmultiplexer response, $t_{k,n}$, is determined by the filter bank design. The transmultiplexer response of the reference filter bank system is illustrated in Table 1-1.

Table 1-1. Transmultiplexer response of the FBMC system using PHYDYAS reference bank.

time sub-ch.	-4	-3	-2	-1	0	1	2	3	4
-2	0	0.0006	-0.0001	0	0	0	-0.0001	0.0006	0
-1	0.0054	j.0429	-0.1250	-j.2058	0.2393	j.2058	-0.1250	-j.0429	0.0054
0	0	-0.0668	0.0002	0.5644	1	0.5644	0.0002	-0.0668	0
1	0.0054	-j.0429	-0.1250	j.2058	0.2393	-j.2058	-0.1250	j.0429	0.0054
2	0	0.0006	-0.0001	0	0	0	-0.0001	0.0006	0

It can be seen that the effect of subchannel k on the second adjacent subchannels ($k-2$, $k+2$) is very small. In the time direction, the effect of sample at time n extends to the range $n-4$ to $n+4$, due to the overlapping factor of 4.

The non-orthogonality (due to NPR design) can be seen in the samples $(k \pm 2, n \pm 2)$, $(k, n \pm 2)$, which are quite small in magnitude. The resulting background noise of the system is at the level of $\sigma_b^2 = -65\text{dB}$ assuming that the subchannel signal variance is 1.

2 General scope of WP3: Equalization

The objective of WP3 is to define the processing needed at the receiver for equalization and demodulation in an FBMC system, keeping in mind the scalability requirements for multi-user scenarios. The main points in task 3.1 are all directly related to the equalization issue. They concern the design of the equalizer structure best suited to the considered modulation and environment, the study of pilot configurations and amount of pilots needed for estimation and synchronization purposes, and finally the efficient demodulation of OQAM signals. All these points are studied and discussed in the present deliverable.

Equalization is an essential part of the processing at the receiver, necessary to take care of the multi-path nature of the transmission channel. One of the big advantages of FBMC is that it allows simple per-subcarrier equalization, just as in OFDM, without the loss of bandwidth efficiency associated with the cyclic prefix. FBMC relies on the selectivity of the filter bank filters to mitigate the intercarrier interference and ensures that each subcarrier is narrow enough to have a virtually flat channel inside its bandwidth. Several comments are important regarding the equalization issue for FBMC. They are summarized below.

Number of subcarriers: It is necessary to choose a sufficient number of subcarriers, so that each individual subcarrier has a narrow bandwidth and can be equalized easily, with a limited number of taps. In addition, a high number of subcarriers provide a higher resolution in terms of spectrum sensing, and an increased versatility for frequency division among users for instance. On the downside, the complexity increases with the number of subcarriers, and the sensitivity to synchronization issue is also increased. The burst truncation effects (see D2.1) are also more difficult to mitigate when using higher number of subcarriers. Based on all these considerations, and in order to enhance the compatibility with current WiMAX systems, it has been chosen to work with 1024 subcarriers as benchmark. This appears (see results below) to be sufficient to have a very simple 1-tap equalization on typical channels.

OQAM demodulation: The particular format of the OQAM modulation, transmitting alternatively on the real and imaginary part, allows to take full advantage of the bandwidth and transmit at high bandwidth efficiency. Equalization needs however to make sure that no intersymbol is generated between the real and imaginary parts due to the channel frequency selectivity. Again, with 1024 subcarriers on mildly selective channels, the resulting intersymbol interference is usually low. For more selective channels, equalizers with several taps need to be designed. The easiest way to handle the OQAM demodulation, with linear equalizers, is described below (Section 4). Even though the obtained results are already satisfactory, further improvements could be possible, using non linear receivers, to take into account the information contained in the complementary (imaginary or real) part of each received symbol. This study is left for future work.

Fractional sampling: The symbol duration is here denoted by T (see system description). As the symbols are actually generated at $T/2$ due to the OQAM modulation format, it is natural for the

equalizer to work at the fractional sampling $T/2$. It has the advantage of corresponding to the approximate bandwidth of each individual filter of the filter bank, which means that no aliasing is generated when performing the equalization at the fractional sampling. For this reason, all the equalizers considered here work at this rate. It is theoretically possible to perform equalization at the symbol rate $1/T$ when using multi-band equalizers, but it does not bring any specific advantage, so it will not be considered here.

Channel estimation: Most equalizer designs are based on the assumption that some channel estimate is available. It is thus necessary to investigate accurate channel estimation. Different methods using pilot symbols are presented in Section 3. Note that it is of course necessary both to estimate the channel at the initialization, as well as track the changes of the channel due to the mobility in a wireless environment.

Adaptivity: While channel estimation based on pilots is necessary for a fast initialization, the tracking can be performed using adaptive methods that do not necessarily require an explicit estimate of the channel. Blind (or decision-directed) techniques can even help to further reduce the amount of required pilots and increase the net data rate. As a first step towards this direction, a simple LMS algorithm is described below.

Synchronization issues: Similarly to the issue of channel estimation, it is of course necessary to track both the CFO (carrier frequency offset) and the symbol timing during transmission. The initialization is discussed in deliverable D2.1. The tracking and compensation of the CFO is discussed in Section 4. Part of the tracking of the (symbol) timing can be performed thanks to the adaptation of the equalizer. However, a single tap equalizer cannot compensate for any timing error, so some coarse tracking of the timing would be needed in that case. This is studied in Section 4. An equalizer with several taps has tracking capability, allowing to relieve the precision constraints on the tracking scheme, so it might be interesting to slightly increase the equalizer complexity for this reason. A possible coarse tracking scheme is presented in deliverable D2.1.

Multi-user schemes: One of the main advantages of the FBMC system is that it allows an easy multiple-access scheme by allocating different sets of subcarriers to different users. A frequency guard interval of one subcarrier is sufficient to separate the users, thanks to the selectivity of the filters. Each user can apply per-subcarrier equalizers on its own subcarriers without any modification so the equalization remains very simple. The CFO and timing compensation bring a more difficult issue, particularly in uplink. Each user has now a different CFO and timing, and it is not possible to compensate for all of them together before the analysis filter bank. It is of course possible to force some synchronization of the different users, with feedback mechanisms, as it is done in OFDM. However, it would offer much more flexibility to the system to allow unsynchronised users to transmit simultaneously and this will be investigated during the next semester. The combination of single carrier modulation and multicarrier modulation in uplink will also be studied.

Equalization structures: Different possible equalization structures will be described, analyzed and compared below. The obtained performance will also be compared to OFDM in order to confirm the expected gain. Here are the different equalizer structures investigated.

- The basic equalization is a single-tap per sub-carrier equalizer. It is based on channel estimation and will generally just invert the channel at the center frequency of the corresponding subcarrier. It is working well in mildly selective channels as long as the number of subcarriers is sufficient.
-

- The first enhancement is to have a multiple taps (per-subcarrier) equalizer, typically working at $T/2$, and usually limited to 3-5 taps. It allows compensating for more selective channels, and for timing errors. There are several possible design criteria:
 - A low-complexity solution is based on frequency interpolation (also called frequency sampling). Its principle is to use the channel estimation at the center frequencies of each subcarrier, and then interpolate in order to provide an approximate frequency response inside each subchannel, that can directly be inverted to provide a suitable equalizer.
 - The MMSE criterion can be used, based on channel estimation. This is relatively complex as it requires the computation of the correlation matrix as well as its inversion. A simplification will be proposed that slightly decreases the complexity associated with the computation of the matrix.
 - Finally, it is also possible to use adaptive methods that do not rely directly on channel estimation.
- When it is needed to cope with very selective channels, the equalizer can be further improved by using a multi-band equalizer, as opposed to per-subcarrier equalizer. The idea is to use the outputs of the analysis filter bank corresponding to adjacent subcarriers instead of using only the output of the corresponding subcarrier, as these outputs also contain some useful power.
- Previous work on the topic [25] has shown that it might be interesting, in some situations, to combine the per-subcarrier equalizer with a pre-processing before the analysis filter bank, which is thus common to all subcarriers. This is however only interesting when using long equalizers with very selective channels, and does not apply to the wireless environment considered here. In addition, this method is not well suited to a multi-user uplink scenario where the channels coming from the different users might be completely different. For these reasons, this type of equalizers will not be considered.

As a general comment, it is more efficient for all these operations (equalization, compensation of synchronization errors, ...) to be performed in the frequency domain (at the output of the analysis filter bank) on a per-subcarrier basis in order to take advantage of the selectivity of the filter bank. This also allows for some more flexibility regarding the multi-user scenario.

The rest of the deliverable is structured as follows. In Section 3, channel estimation is investigated based on the use of pilots. In particular, the pilot scheme is modified in order to take into account the particular case of the OQAM modulation. In Section 4, the different types of equalizer are presented and their performances are evaluated. The compensation of synchronization errors is also discussed in that section. Section 5 presents a more detailed comparison of the different equalization structures in a WiMAX scenario, and gives a few conclusions regarding the choices to be made.

3 Channel estimation

In this chapter, we investigate channel estimation methods for FBMC systems. The literature on this topic is fairly limited, [6]-[8], and no straightforward solutions are available. The focus is here mostly on data-aided methods, i.e., the channel estimation is based on known transmitted symbols, which may appear either in the form of preambles or pilots. A preamble is a special multicarrier symbol, in the beginning of the transmission frame, which is designed for synchronization and channel estimation purposes and does not carry user data. In the multicarrier literature, pilots refer to known training symbols, which are scattered among data symbols at predetermined subcarrier symbol positions, following patterns which are characteristic to each particular system.

Due to the use of OQAM subcarrier modulation, the use of pilots in FBMC systems is not as straightforward as in OFDM. Two different pilot schemes have been presented in [8] and [9] for channel estimation purposes. The latter approach can also be used for constructing preambles. In this chapter, we consider both schemes in the context of the PHYDYAS reference filter bank and in WiMAX-like pilot configurations.

First, in Section 3.1, we utilize the idea of [8] to construct FBMC pilots which can be used basically in the same way as pilots in OFDM. We refer to this scheme as the auxiliary pilot scheme. Certain simplifications in calculations related to the pilot construction are discussed. In Section 3.2, we discuss possibilities to apply the auxiliary pilot scheme with WiMAX (802.16e)-like pilot patterns. In Section 3.3, the scheme of [9] is investigated.

The auxiliary pilot scheme is investigated in the PHYDYAS deliverable D2.1 [9] in the carrier frequency offset (CFO) and symbol timing estimation context. To provide sufficient background for both deliverables, the contents of Sections 3.1 and 3.2 are mostly repeated in both documents.

3.1 Auxiliary pilot scheme

In an OQAM-FBMC system, either real or imaginary parts of the complex subcarrier symbols are used for data transmission in a staggered fashion. As discussed in Section 1, when a real (imaginary) part of a subcarrier symbol is used, the unused imaginary (real) part is, at the receiver, a fairly complicated function of surrounding data symbols. In the following, we refer to these two parts of the complex symbols as primary and secondary parts, respectively. In the case of PR filter bank system, there is no crosstalk among the primary parts (or secondary parts) themselves. In the case of near NPR filter banks, like the PHYDYAS reference bank, the crosstalk effects between the primary parts are small enough to be neglected.

The nature of FBMC systems makes it impossible to construct pilot symbols for channel estimation and synchronization purposes in the same way as in OFDM. The approach taken in [8] is based on the observation that it is enough to select one of the subcarrier symbols close to a pilot symbol as an associated auxiliary pilot. Adjusting the primary part of the auxiliary pilot depending on the surrounding data symbols, the secondary part of the actual pilot can be forced to take any desired value. For example, the secondary part of the complex pilot symbol can be forced to zero. Utilizing this idea, pilots can be used in FBMC systems in a similar way as in OFDM. It should be noticed that the relative pilot overhead using this idea is the same as the pilot overhead in OFDM, i.e., for each pilot, one OQAM is used in the FBMC case and one QAM symbol in the OFDM case. However, in the presented auxiliary pilot scheme, there are several alternatives in choosing the

location of the auxiliary pilot. It is not necessary to place the pilot and auxiliary pilot in the same OQAM symbol.

In case of a frequency-selective channel and sufficiently narrow subcarrier spacing, the pilot would suffer from attenuation and phase rotation directly related to the channel. Simple estimation of the received pilot amplitude and phase yields estimates for the channel's amplitude and phase for that frequency bin.

Based on Section 1.2.4, looking at the AFB output samples in the receiver in case of an ideal channel, the symbol (pilot) of interest at (k_p, n_p) , can be expressed as:

$$x_{k_p, n_p} = \sum_{(k, n) \in \Omega_{k_p, n_p}} d_{k, n} \theta_{k, n} t_{k_p - k, n_p - n}, \quad (11)$$

where Ω_{k_p, n_p} is the set of neighboring symbol positions which have a significant effect on the symbol at (k_p, n_p) . Especially, the secondary part of the symbol is

$$u_{k_p, n_p} = \sum_{(k, n) \in \Omega_{k_p, n_p}} d_{k, n} \text{Im} \left[\theta_{k - k_p, n - n_p} t_{k_p - k, n_p - n} \right] = \sum_{(k, n) \in \Omega_{k_p, n_p}} d_{k, n} \hat{t}_{k_p - k, n_p - n}, \quad (12)$$

where

$$\hat{t}_{k, n} = \text{Im} \left[(-j)^{k, n} t_{k, n} \right], \quad (13)$$

whereas the primary part is the original primary value, d_{k_p, n_p} , plus some additive interference which can be assumed to be negligible.

The transmultiplexer response $t_{k, n}$ is known from the filter bank design. If the prototype filter is designed with good frequency selectivity and roll-off factor $\alpha \leq 1$, the range includes k_p and both adjacent subcarriers, $k_p - 1$ and $k_p + 1$, in the frequency dimension. The range of n is $[n - K, n + K]$, e.g., 7 or 9 subcarrier samples with the typical overlapping factors (K) of 3 or 4.

The auxiliary pilot position is denoted in the following as (k_a, n_a) and the auxiliary pilot is assumed to be chosen in such a way that the secondary part of the pilot sample becomes zero. This can be achieved by choosing

$$d_{k_a, n_a} = - \frac{\sum_{\substack{(k, n) \in \Omega_{k_p, n_p} \\ (k, n) \neq (k_p, n_p) \\ (k, n) \neq (k_a, n_a)}} d_{k, n} \hat{t}_{k_p - k, n_p - n}}{\hat{t}_{k_p - k_a, n_p - n_a}} \quad (14)$$

We notice that a small absolute value of $\hat{t}_{k_p - k_a, n_p - n_a}$ results in large magnitude of the auxiliary pilot, which wastes transmission energy and is expected to be bad for the peak-to-average power ratio (PAPR) of the transmitted waveform. Thus it is preferable to choose the auxiliary pilot in such a way that the magnitude of the denominator is maximized. In typical filter bank designs, including the PHYDYAS reference filter bank, the choice for the auxiliary pilot is the sample immediately preceding or following the pilot, i.e., $(k_p, n_p - 1)$ or $(k_p, n_p + 1)$.

Performance evaluation

Figure 3-1-1 shows two alternative definitions for the Ω_{k_p, n_p} . The smaller window includes 11 subcarrier samples (excluding the pilot and auxiliary pilot) and the larger one 17 samples. The values of \hat{t}_{k_p, n_p-1} and \hat{t}_{k_p, n_p+1} are equal to 0.5644. This value is about double compared to the second largest magnitude in Ω_{k_p, n_p} .

For the preliminary simulations, we have considered a configuration of one pilot regularly placed in a group of 8 subcarriers. With this configuration, we show simulation based results on the interference and also on the PAPR when the data in the data subcarriers consists of QPSK symbols. The average power level of the auxiliary pilots with this configuration is somewhat higher than 3 dB above the pilot power level.

In case of ideal channel model, the complex residual interference in the pilot values is the joint effect of the use of NPR filter bank and the use of limited window size in the auxiliary pilot calculations. Figure 3-1-2 presents the histogram of the amplitude of the residual interference in the case of the wider window. The shape clearly indicates a non-biased Gaussian noise-like distribution. In the case of the narrower window, the distribution is more quantized, but probably higher order modulation would smoothen the shape.

0	0.0006	-0.0001	0	0	0	-0.0001	0.0006	0
0.0054	-0.0429i	-0.1250	0.2058i	0.2393	-0.2058i	-0.1250	-0.0429i	0.0054
0	-0.0668	0.0002	0.5644	1.0000	0.5644	0.0002	-0.0668	0
0.0054	0.0429i	-0.1250	-0.2058i	0.2393	0.2058i	-0.1250	0.0429i	0.0054
0	0.0006	-0.0001	0	0	0	-0.0001	0.0006	0

(a)

0	0.0006	-0.0001	0	0	0	-0.0001	0.0006	0
0.0054	-0.0429i	-0.1250	0.2058i	0.2393	-0.2058i	-0.1250	-0.0429i	0.0054
0	-0.0668	0.0002	0.5644	1.0000	0.5644	0.0002	-0.0668	0
0.0054	0.0429i	-0.1250	-0.2058i	0.2393	0.2058i	-0.1250	0.0429i	0.0054
0	0.0006	-0.0001	0	0	0	-0.0001	0.0006	0

(b)

Figure 3-1-1. Auxiliary pilot calculation windows for PHYDYAS reference bank.

(a) Narrow window. (b) Wider window.

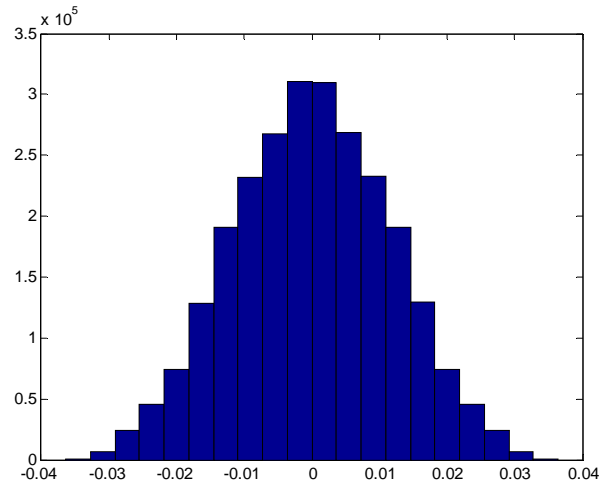


Figure 3-1-2. Histogram of residual pilot interference with wider window.

Assuming the imaginary noise to be Gaussian, the residual interference is at the level of -17.8 dBr with smaller window and at -38.7 dBr with wider window, considering the real pilot symbol amplitude of 1 as the reference. Then it is obvious that the wider window should be utilized.

From the peak to average power point of view, the effect of the auxiliary pilot seems moderate, at least in the 10000 realization sets that we performed, as can be seen in Figure 3-1-3.

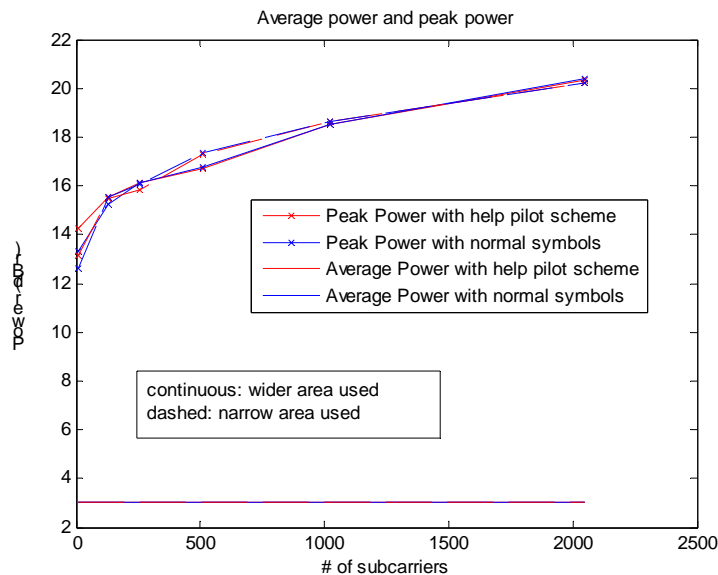


Figure 3-1-3. Effect of auxiliary pilots on the PAPR with PHYDYAS reference bank.

The performance of the auxiliary pilot scheme in channel estimation is shown in Figure 3-1-4 considering both windows. A clear conclusion from this experiment is that the wider window provides sufficient performance, as far as the quality of the pilots is considered, but with narrower window, the performance is questionable.

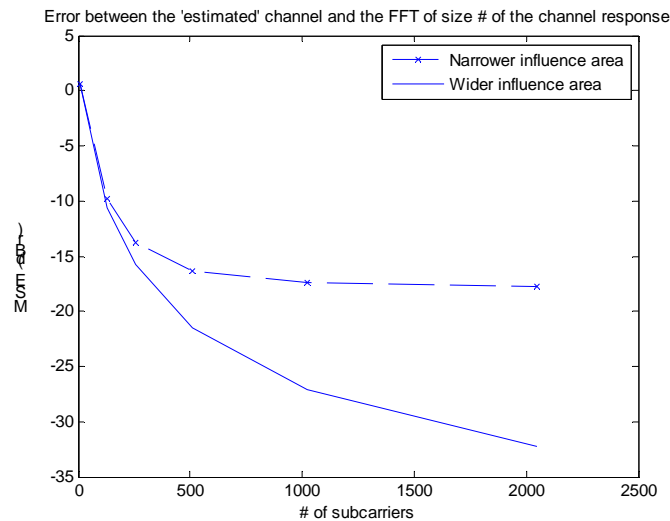


Figure 3-1-4. Channel estimation MSE with PHYDYAS reference bank using the auxiliary pilot scheme with the two alternative windows.

3.2 Application of auxiliary pilot scheme to WiMAX pilot structures

The target of PHYDYAS is to develop WiMAX-like air-interface using the FBMC approach. Thus, it is natural to consider direct adaptation of the 802.16e pilot patterns to the FBMC model.

Let us consider first the pilot structure used in the *adaptive modulation and coding* (AMC23) mode, both in uplink and downlink. The AMC23 OFDM pilot pattern is shown in Figure 3-2-1(a). Here each OFDM symbol corresponds to two consecutive subcarrier samples in the FBMC model. It can be seen that auxiliary pilot calculations can be done without difficulties using the PHYDYAS reference filter bank and the principles described above. Regular pilot structure can be easily used. The natural choice is to choose the auxiliary pilot to be in the same OQAM symbol with the pilot.

In the downlink *partial usage of subchannels* (PUSC) mode, illustrated in Figure 3-2-1(b), there are some difficulties. If a regular placement of auxiliary pilots is adopted and the wider window is used in the auxiliary pilot calculations, there will be cases where an auxiliary pilot is in the window of another auxiliary pilot. In this case, recursive calculation of auxiliary pilots would be required, which may be somewhat inconvenient. However, by using a slightly modified pilot scheme, this difficulty can be avoided, and each of the auxiliary pilots can be calculated independently of the others. In the modified scheme, the order of pilot and auxiliary pilot is exchanged in every second instance within a subcarrier, as illustrated in Figure 3-2-2.

The uplink-PUSC (see Figure 3-2-1(c)) is even trickier due to the higher density of pilots. Even with smart positioning of the pilots and help pilots, the calculation of each help pilots requires the solving of a equation system of 4 equations with 4 unknowns. This makes the auxiliary pilot calculations more complicated in the uplink-PUSC mode.

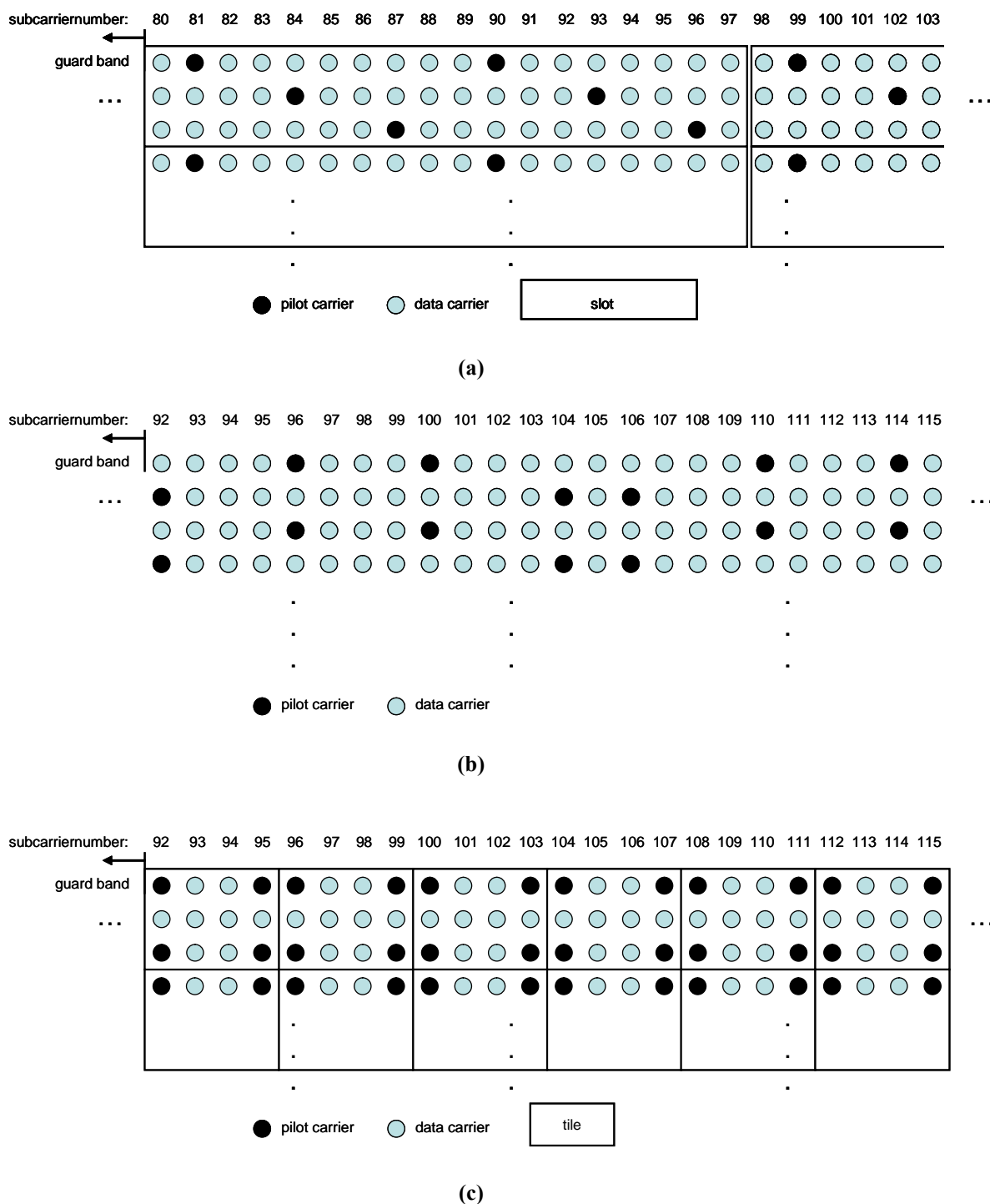


Figure 3-2-1. Pilot and data allocations in WiMAX (OFDM). (a) AMC23 (b) DL PUSC (c) UL PUSC

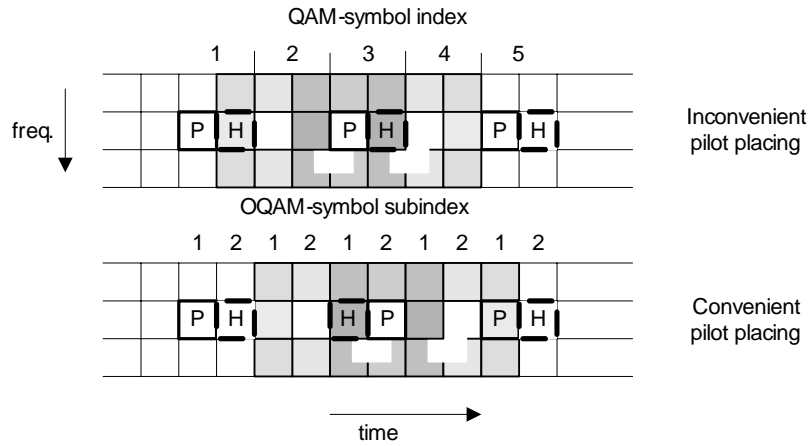


Figure 3-2-2. Alternative pilot and data allocations for FBMC with DL PUSC like pilot pattern.

3.3 Preamble-Based Schemes

In this subsection, the methods of preamble-based OFDM/OQAM channel estimation proposed by [8][15] are considered. The preambles proposed therein are then adapted to the WiMAX standard structure for pilot-aided channel estimation, for the sake of backward compatibility. Simulation results from both preamble- and pilot-aided estimation are provided.

In the FBMC/OQAM approach, the channel estimation issue is different of that in conventional CP-OFDM. The reason is that, as already explained, the sought channel frequency response values are complex whereas the training input is real. Moreover, the AFB output samples also contain imaginary contributions from neighbouring times and frequencies. Under the assumptions of good time-frequency localization for the employed prototype filter and relatively low frequency selectivity for the channel, [8] came up with two preamble-based methods for channel estimation in FBMC/OQAM systems. The first method, Pairs of Pilots (POP), relies on simple algebraic relations for the input / output samples in two (in practice consecutive) time instants. The second one, Interference Approximation Method (IAM), instead aims at approximating the *intrinsic* imaginary interference from neighboring pilots and hence constructing complex pilots, to accommodate the complex channel.

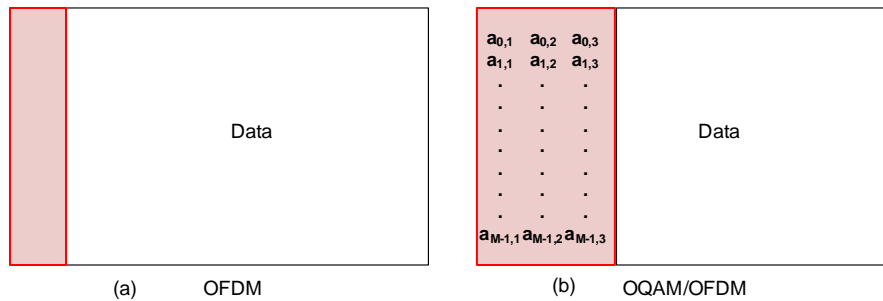


Figure 3-3-1. Preambles in (a) OFDM and (b) OFDM/OQAM systems [14].

Recall that simple frequency-domain per-subcarrier channel estimation in CP-OFDM consists of dividing the received sample at a certain frequency-time point (k_0, n_0) with the complex pilot transmitted at that position (see Fig. 3-3-1(a)). Namely, with $n_0 = 0$ (as in Fig. 3-3-1(a)),

$$\hat{H}_{k_0,0} = \frac{y_{k_0,0}}{S_{k_0,0}} \quad (15)$$

In the OFDM/OQAM system, under the previously mentioned assumptions, the output of the m th analysis filter at time n can be written as¹ [8]:

$$y_{k,n} = H_{k,n} (d_{k,n} + ju_{k,n}) + \eta_{k,n} \quad (16)$$

where $d_{k,n}$ is the corresponding input symbol (primary part) and $ju_{k,n}$ denotes the intrinsic interference from the surrounding time-frequency points (the secondary part). The latter is built out of the contributions of the neighboring points [8]:

$$u_{k,n} = \sum_{(p,q) \neq (0,0)} d_{k,n} \langle p \rangle_{k+p,n+q}^{p,q} \quad (17)$$

where, for properly designed prototype filter $p(m)$,

$$\langle p \rangle_{k+p,n+q}^{k,n} \triangleq -j \langle p_{k+p,n+q} | p_{k,n} \rangle = -j \sum_m p_{k+p,n+q}(m) p_{k,n}^*(m)$$

is real. With a well localized filter $p(m)$, only the first-order neighbors (i.e., $p, q \in \{-1, 0, 1\}, (p, q) \neq (0, 0)$) significantly contribute to $u_{k,n}$. Again, $H_{k,n}$ is assumed to be (almost) invariant in the neighborhood covered by $u_{k,n}$.

3.3.1 Estimation using the Pairs of Pilots (POP) method

This method aims at computing a channel estimate by using (16) at two different (in practice consecutive) time instants, n_1, n_2 , to construct a system of equations for the real and imaginary parts of $H_{k,n}$. Let us describe this method in the equivalent way suggested in [12]. Denote by $W_{k,n} = 1/H_{k,n}$ the corresponding zero forcing (ZF) equalizer coefficients. Then, assuming $n_1 = 0, n_2 = 1$ (see Fig. 3-3-2(a)) and *neglecting* the noise, one can write, for even k :²

$$\begin{aligned} y_{k,0} W_{k,0} &= d_{k,0} + ju_{k,0} \\ y_{k,1} W_{k,1} &= u_{k,1} + jd_{k,1} \end{aligned} \quad (18)$$

Then,

$$\begin{aligned} y_{k,0}^R W_{k,0}^R - y_{k,0}^I W_{k,0}^I &= d_{k,0} \\ y_{k,1}^I W_{k,1}^R + y_{k,1}^R W_{k,1}^I &= d_{k,1} \end{aligned}$$

and, recalling that $W_{k,0} \cong W_{k,1}$,

¹ This holds for odd $k+n$. For even $k+n$, we would similarly have $y_{k,n} = H_{k,n} (u_{k,n} + jd_{k,n}) + \eta_{k,n}$.

² Analogous statements hold for odd k .

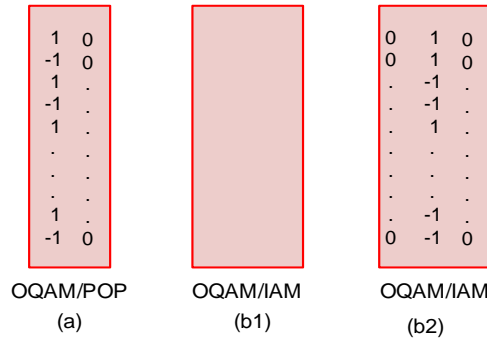


Figure 3-3-2. Preambles for channel estimation using the (a) POP and the (b1, b2) IAM schemes [8].

$$\begin{bmatrix} y_{k,0}^R & -y_{k,0}^I \\ y_{k,1}^I & y_{k,1}^R \end{bmatrix} \begin{bmatrix} W_{k,0}^R \\ W_{k,0}^I \end{bmatrix} = \begin{bmatrix} d_{k,0} \\ d_{k,1} \end{bmatrix}$$

Hence,

$$\begin{bmatrix} W_{k,0}^R \\ W_{k,0}^I \end{bmatrix} = \frac{1}{y_{k,0}^R y_{k,1}^R + y_{k,0}^I y_{k,1}^I} \begin{bmatrix} d_{k,0} y_{k,1}^R + d_{k,1} y_{k,0}^I \\ -d_{k,0} y_{k,1}^I + d_{k,1} y_{k,0}^R \end{bmatrix}$$

More compactly:

$$W_{k,0} = \frac{d_{k,0} y_{k,1}^* + j d_{k,1} y_{k,0}^*}{\text{Re}(y_{k,0} y_{k,1}^*)} \quad (19)$$

In the preamble proposed in [8] (Fig. 3-3-2(a)), $d_{k,1} = 0$ and, for even k , $d_{k,0} = 1$; thus,

$$W_{k,0} = \frac{y_{k,1}^*}{\text{Re}(y_{k,0} y_{k,1}^*)}$$

An advantage of the POP scheme, besides its simplicity, is that it does not explicitly depend on the employed prototype filter. However, it must be emphasized that the above derivation only holds when noise is negligible. One can see that (see [8]), in the presence of noise, the method can have unpredictable performance since the degree of the noise enhancement in general also depends on unknown (hence uncontrollable) data.

3.3.2 Estimation using the Interference Approximation Method (IAM)

If the interference $u_{k,n}$ is only due to the immediate neighbors of (k,n) and these correspond to *training* (hence known) symbols, then one can compute an approximation of this interference. This can then be used to construct the complex so-called *pseudo-pilots* $x_{k,n} = d_{k,n} + j u_{k,n}$ and subsequently use them to get a channel estimate as in CP-OFDM:

$$\hat{H}_{k,n} = \frac{y_{k,n}}{x_{k,n}} \quad (20)$$

This method is called (for obvious reasons) the Interference Approximation Method (IAM) and requires that all input symbols in the immediate neighborhood of (k, n) be known. This implies that 1.5 complex symbols are required for training, representing an increased (though not significantly) overhead compared to CP-OFDM (Fig. 3-3-2(b1, b2)) (the training would need to extend over more than three time instants for less well localized filters).

Noise was not explicitly considered in the above scheme. Writing (20) out,

$$\hat{H}_{k,n} = H_{k,n} + \frac{\eta_{k,n}}{d_{k,n} + ju_{k,n}}, \quad (21)$$

one can see that the pseudo-pilots should be so chosen as to minimize the effect of the noise term. In [8] it is proposed that these be chosen so as to have maximum magnitude. To this end, the surrounding training symbols should be such that all terms in (17) have the same sign so that they add together³. It turns out that a simple preamble training scheme that (seems to) reach this goal, with QPSK modulation, consists of zeros at the instants 0 and 2 and $1, 1, -1, -1, \dots, 1, 1, -1, -1$ for $d_{k,1}, k = 0, 1, \dots, M-1$, as in Fig. 3-3-2(b2).

3.3.3 Simulation Results with Preamble-Aided Channel Estimation

We have simulated the above methods using the PHYDYAS reference filter bank with $M = 1024$ and $K = 4$. The channel was modeled as block fading Veh-A, with zero mobility and AWG noise. The input was QPSK modulated. CP-OFDM was also considered in the experiments. The training for all methods was as outlined above [8]. Perfect synchronization was assumed. 200 frames of 53 complex symbols each were transmitted. Fig. 3-3-3 shows the (normalized) channel estimation MSE versus bit SNR. Note that the useful bit SNR (E_b / N_0) takes into account the energy wasted in the CP for CP-OFDM. A more significant improvement over CP-OFDM is expected for channels of a larger delay spread.

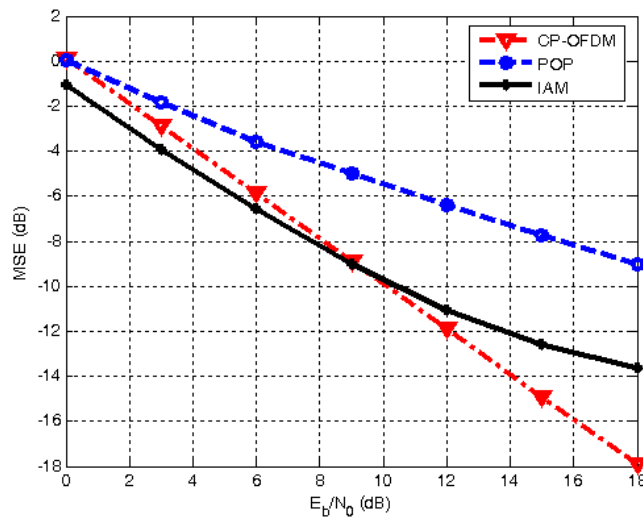


Figure 3-3-3. Normalized MSE for POP and IAM preamble-based schemes. CP-OFDM is also included.

³ It must be noted here that how large $|u_{k,n}|$ can be also depends on the choice of the prototype filter [8][13].

The POP method is seen to be always outperformed by CP-OFDM. This should not be unexpected in view of the fact that, as pointed out above, with POP one cannot control the effect on the noise. One can see that IAM performs, in general, better than CP-OFDM (recall here that OFDM/OQAM does not employ any kind of guard interval). Notice also that, as suggested by this example (and others), IAM exhibits an error floor at high SNR's. The BER results for ZF per-subcarrier equalization (with uncoded QPSK input) are shown in Fig. 3-3-4.

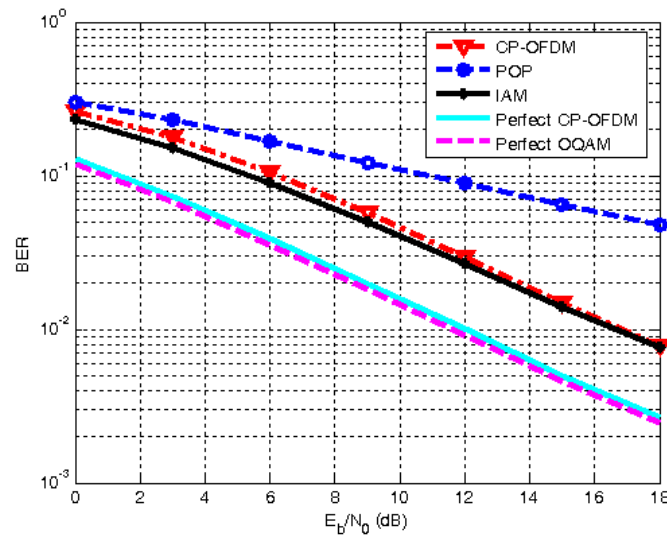


Figure 3-3-4. BER results for POP and IAM methods, and for the CP-OFDM system. The results with perfect channel knowledge are also included.

3.3.4 Adaptation to the DL PUSC communication mode

The preambles proposed in [8] can be also translated to the WiMAX pilot allocation scheme [17], for pilot-aided channel estimation. The downlink (DL) partial usage of subcarriers (PUSC) configuration for data and pilot allocation in the CP-OFDM system is recalled in Fig. 3-3-5(a), where an average of one pilot per eight subcarrier symbols is used.

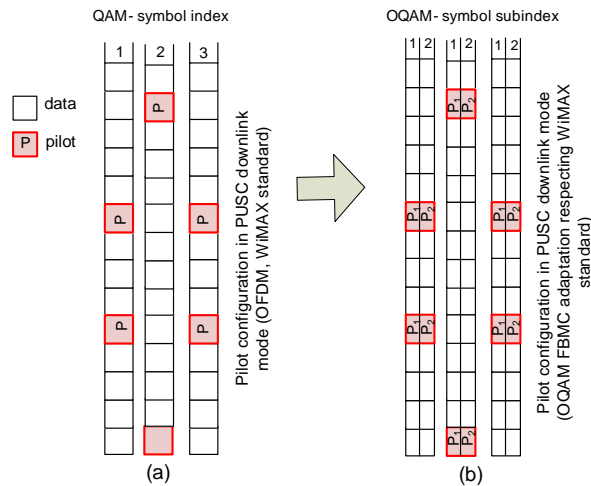


Figure 3-3-5. Pilot allocation for (a) OFDM and (b) OFDM/OQAM channel estimation, following the DL PUSC pilot allocation scheme specified in the WiMAX standard [10].

Fig. 3-3-5(b) shows the associated configuration for an OQAM FBMC system. Note that each complex QAM pilot/data sample corresponds to a pair of OQAM samples.

POP Method:

For the POP method the training overhead is similar to that used in CP-OFDM. By adopting the preamble proposed by [8] (see Fig. 3-3-6(b)), pilot allocation can be designed as shown in Fig. 3-3-6(a). Note that to alleviate the risk of high peaks power, the alternation sign $\{\pm 1\}$ of the pilots is respected.

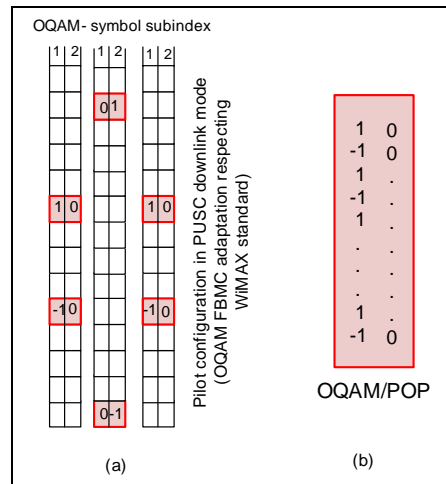


Figure 3-3-6: Pilot allocation for OQAM-FBMC for the POP method and adapted to the DL PUSC configuration.

In the simulation results presented here, the PHYDYAS reference filter bank has been used, with transform size $M = 1024$ and overlapping factor $K = 4$. A signal with 53 multicarrier symbols per frame is analyzed, corresponding to frame duration of 5 ms, as defined in [10]. Carrier and sampling frequencies are set to 10 MHz and 11.2 MHz, respectively. The channel is modelled following the ITU-Pedestrian (A & B), the ITU-indoor (A & B), and ITU-SUI-1 (Fixed Broadband Application) models, with AWGN.

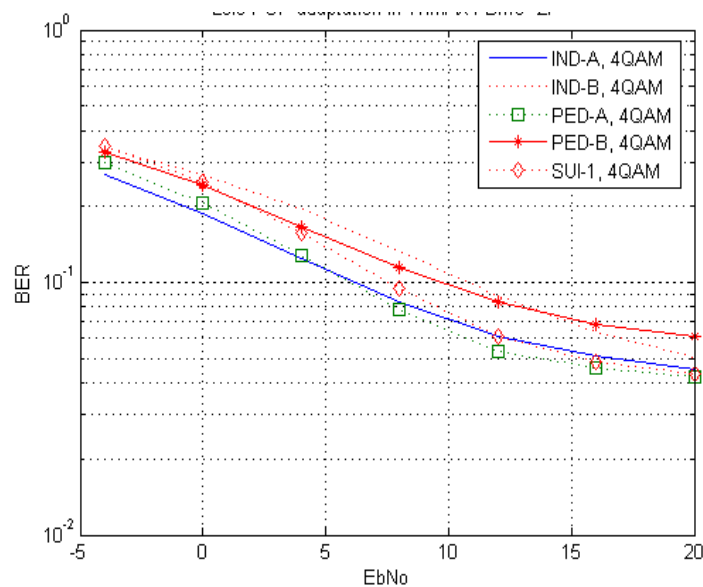


Figure 3-3-7. Adaptation of the POP method to PHYDYAS OQAM-FBMC. BER vs. E_b/N_0 in ITU- Ind-A, Ind-B, Ped (A&B), and SUI-1 channels. DL PUSC, uncoded 4-QAM input, using ZF equalization.

Note that in the DL PUSC scheme, only the pilots, not a preamble as previously, are used in the channel estimation. In our experiments, the signal is assumed to be perfectly synchronized. The interpolation process is carried out using two-dimensional linear surface interpolation (using Matlab function `griddata` as in [18]). The remaining carriers and symbols are estimated using linear extrapolation. The simulations are run over 1100 channel realizations.

We performed a simple channel estimation experiment with the modified POP scheme. Using the ITU- Ind-A, Ind-B, Ped (A&B), and SUI-1 channel models, we performed channel estimation only on the primary pilot symbols. These channel models were chosen because of their low channel variability (quasi-invariant) characteristic. Fig. 3-3-7 presents the results of per-subcarrier ZF equalization, with uncoded 4-QAM input.

IAM Method:

Here a larger number of pilots than in the POP scheme are used (5 pilots at each pilot position) but still lower than in the previous (preamble-based) IAM scheme, where, for each desired time-frequency pilot position, all the surrounding values (eight values) must be reserved for training. In fact, as it is observed in Fig. 3-3-8, we have here a Partial Interference Approximation method, since not all of the contributions to the interference in the pilot $d_{k,n}$ are estimated. Here we are confined to the information provided by the $(k, n-1)$, $(k, n+1)$, $(k-1, n)$, and $(k+1, n)$ frequency-time positions to estimate $u_{k,n}$. Note that the pilots' positions $(k, n-1)$, $(k, n+1)$ are set to zero since they correspond to the most significant contributions to the interference (equal to 0.5644 in the filter bank used here). The interference weights at the frequency-time positions $(k-1, n)$ and $(k+1, n)$ are of a lower value (0.2393). As in the POP case the alternation sign $\{\pm 1\}$ of the pilots is respected.

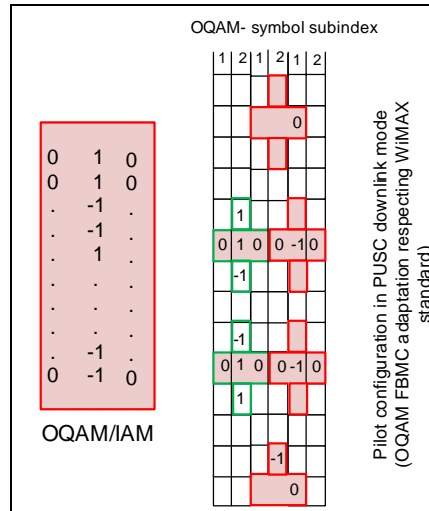


Figure 3-3-8. Pilot allocation for OFDM/OQAM based on the IAM method and adapted to DL PUSC configuration.

The experimental setup is as previously. The channel is modelled as ITU Veh-A, with AWGN.

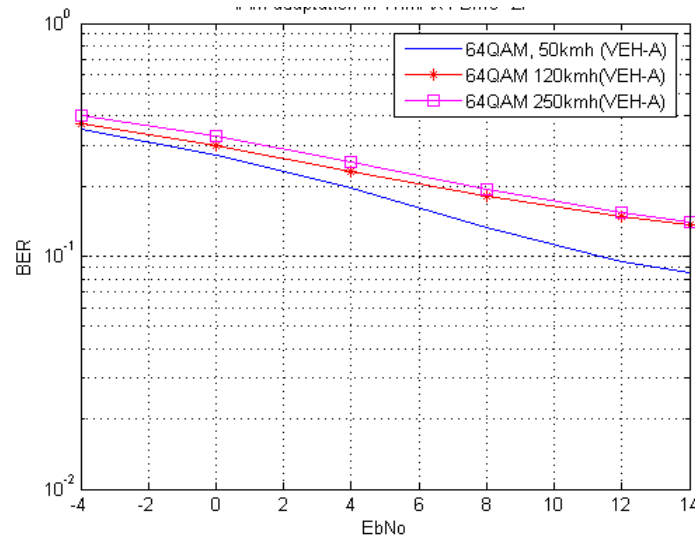


Figure 3-3-9. Adaptation of the IAM method to PHYDYAS OQAM-FBMC. BER vs. E_b/N_0 in ITU Veh-A channel. DL PUSC, uncoded 64-QAM input, using MMSE equalization.

We performed a simple channel estimation experiment with the modified IAM scheme, using only the primary pilot symbols. Fig. 3-3-9 shows the results of MMSE equalization with uncoded 64-QAM and for different mobility speeds.

3.4 Interpolation of pilot-based channel estimates

Regarding interpolation, most of the methods used for the classical OFDM system are also valid for OQAM-FBMC systems. It must be remarked that the optimum interpolation is determined by the channel statistics, such as the delay profile and the Doppler frequency, that are usually difficult to obtain since they depend on the environment and vehicle speed. Hereafter we describe the main classical interpolation filtering.

3.4.1 Two dimensional estimation

The optimal two-dimensional linear channel estimator in terms of *mean-squared error* (MSE) is the 2-D Wiener filter, which can be designed when the statistical properties of the channel are known. This estimator shows high accuracy, but presents a large computational complexity. Therefore, in the design of the channel estimator, a trade off between computational complexity and the performance must be found. Here, the filter weights the received pilot values considering their correlation and noise properties in order to calculate the channel estimates. Firstly channel attenuations at pilot locations must be obtained, and can be obtained using the Least Squares (LS) criterion. Then, the estimated channel attenuation at (k, n) pilot position, is calculated.

3.4.2 Separable filters

2-D filters usually have a large computational complexity, and thus an alternative can be the use of separable filters, using two separate 1-D filters, one in the frequency direction and the other in the time direction. Filtering in the frequency direction is usually performed first; after that, a 1-D filter is applied in the time direction to complete interpolation in all points. This is a common technique to reduce the complexity in multidimensional signal processing, which is applicable also on OQAM-FBMC systems. There is a small performance loss, due to the restriction that the obtained 2-D impulse response must be the outer product of two 1-D filters. Results of this technique are presented in [19].

J.-P. Javaudin *et al.* in [7] have studied two methods for interpolating the estimated coefficients over the whole frame; the low pass filtering with minimum mean squared error (MMSE) criterion (Wiener filtering), and the interpolation with discrete *prolate* sequences. Here, as the length of the Wiener filtering is chosen to fix the computational complexity of the filtering, the Prolate filter is also fixed for the same purpose. For Prolate interpolation, the eigenvectors of the autocorrelation matrix of the impulse response of the channel are calculated. The autocorrelation matrix channel response is a Toeplitz matrix. Results in [7] show that the Prolate interpolator performance improves when the number of Prolate vectors increases, but the optimum is quickly reached. Moreover, when the estimated bandwidth of the frequency response of the channel is too wide, some noise is kept with the useful signal. This means that it is more interesting to choose the narrowest bandwidth possible for a channel because it reduces the number of prolate vectors to take into account. Results from comparing the Wiener filtering with the Prolate filtering in case of low complexity (around 3 complex to real multiplications per carrier for each multicarrier symbol) show that the Prolate interpolation has better performance than Wiener filtering. However, for higher complexity (more than 7 complex to real multiplications per carrier), Wiener filtering has same or lower bit error rate than the Prolate filtering (see Figures 6, 7 and 8 in [7]).

4 Equalizer structures

As discussed above, the most basic equalization structure is the simple one-tap per subcarrier equalizer. Channel estimates obtained for each subcarrier by the pilots methods can be inverted to obtain the corresponding equalizer. Different equalization structures are presented here and compared with the simple 1-tap equalizer. A general comparison of the different equalizers as well as with OFDM performance is presented in Section 5.

First, multiple taps equalizers are investigated. The low complexity method to compute these coefficients is based on “frequency sampling.” Two such techniques are presented in Section 4.1. The more complex multiple-taps MMSE equalizer is then presented in Section 4.2, along with a possible simplification.

In Section 4.3, an even more complex equalizer is presented that makes use of the outputs of the analysis bank corresponding to adjacent bands, in order to help improving the performance. Finally, Section 4.4 is devoted to an adaptive algorithm for computing the equalizer.

The synchronization issue is closely related to the equalization. Sections 4.5, 4.6 deal with the compensation of CFO and timing, respectively, in association with the equalizer.

4.1 Frequency sampling approach

In this section, we present two equalizers based on the frequency sampling approach, with two different methods for computing the equalizer coefficients.

4.1.1 Approach 1

A simple and efficient approach is the frequency sampling technique, which allows to equalize the sub-channel frequency response at a number of frequencies equal to the number of coefficients of the equalizer.

The measurement of the transmission channel response with the frequency step Δf equal to the sub-channel spacing produces the values $C(i)$, with i the sub-channel index. In the single coefficient case, the equalizer coefficient is just $EQ(i) = 1/C(i)$. If several coefficients are used, they are computed from several values of the channel frequency response. The case of 3 coefficients is detailed below.

Since the AFB is oversampled by the factor 2, the sub-channel sampling frequency is $2\Delta f$. With 3 coefficients, in order to adequately cover the bandwidth of sub-channel i , the following equalization frequencies are chosen: the center frequency $i\Delta f$ and the two intermediary frequencies $(i \pm 1/2)\Delta f$. Then, two interpolated values, $EQ1$ and $EQ2$, as shown in Figure 4-1-1, have to be computed.

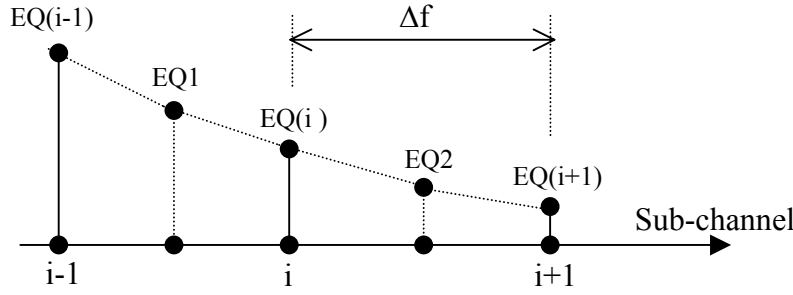


Fig.4-1-1. Frequency response of the sub-channel equalizer.

The coefficients of the equalizer are computed in such a manner that its frequency response goes through the values EQ1, EQ(i) and EQ2. Then, the frequency sampling step is $\Delta f / 2$, which leads to the number of samples $2 \Delta f / (\Delta f / 2) = 4$. Thus, one value is unknown and it is designated by A.

Now, the equalizer coefficients are obtained with the help of the inverse Fourier transform of the set $\{A, EQ1, EQ(i), EQ2\}$. These values are denoted $\{h_0, h_1, h_2, h_3\}$. The center coefficient h_0 is surrounded by the coefficients $h_{-1} = h_3$ and h_1 . If the equalizer is limited to 3 coefficients, the coefficient h_2 must be set to zero which determines the unknown A through the relation:

$$A - EQ1 + EQ(i) - EQ2 = 0$$

Next, the center coefficient is

$$h_0 = A + EQ1 + EQ(i) + EQ2$$

If a linear interpolation is chosen, which implies that the interpolated values are

$$EQ1 = [EQ(i-1) + EQ(i)] / 2 \text{ and } EQ2 = [EQ(i) + EQ(i+1)] / 2,$$

the set of coefficients is

$$\begin{aligned} h_0 &= [EQ(i-1) + EQ(i+1) + 2EQ(i)] / 4 \\ h_1 &= [EQ(i-1) + EQ(i+1) - 2EQ(i) + j(EQ(i-1) - EQ(i+1))] / 8 \\ h_{-1} &= [EQ(i-1) + EQ(i+1) - 2EQ(i) - j(EQ(i-1) - EQ(i+1))] / 8. \end{aligned}$$

In order to take into account the particularities of the OQAM technique, the signs of the coefficients h_1 and h_{-1} have to be changed as a function of the sub-channel index i , which is achieved through a multiplication by the factor $(-1)^i$.

4.1.2 Approach 2

In this approach, the subchannel equalizers are designed using a frequency sampling technique based on frequency domain channel estimates. The principal idea is to optimize / solve the equalizer coefficients in such a manner that the frequency response of the designed filter is forced to take the given target values (i.e., transfer function goes through pre-determined points) at a set of considered frequency points within a subchannel [6]. This design scheme enables frequency selective subchannel processing. Typically, a frequency grid where a number frequency points is two times the number of subchannels is used in the design. In this case, subchannel equalizers designed based on one, two or three target points per subchannel can be derived. In general, also higher number of points can be used in the design, however, with the expense of somewhat more complex equalizer structures and more demanding derivation of the optimized filter coefficients. Between the given set of frequency points, the equalizer response is approximating the optimal frequency selective response. For example, in the case of zero-forcing (ZF) criterion, this optimal response is the inverse of the channel transfer function. The level of approximation error depends on the level of frequency selectivity within subchannel bandwidth. Moreover, it should be noted that this approach gives some degrees of freedom in the system design with respect to size of the filter bank (number of subchannels) and the order of the subchannel processing performed.

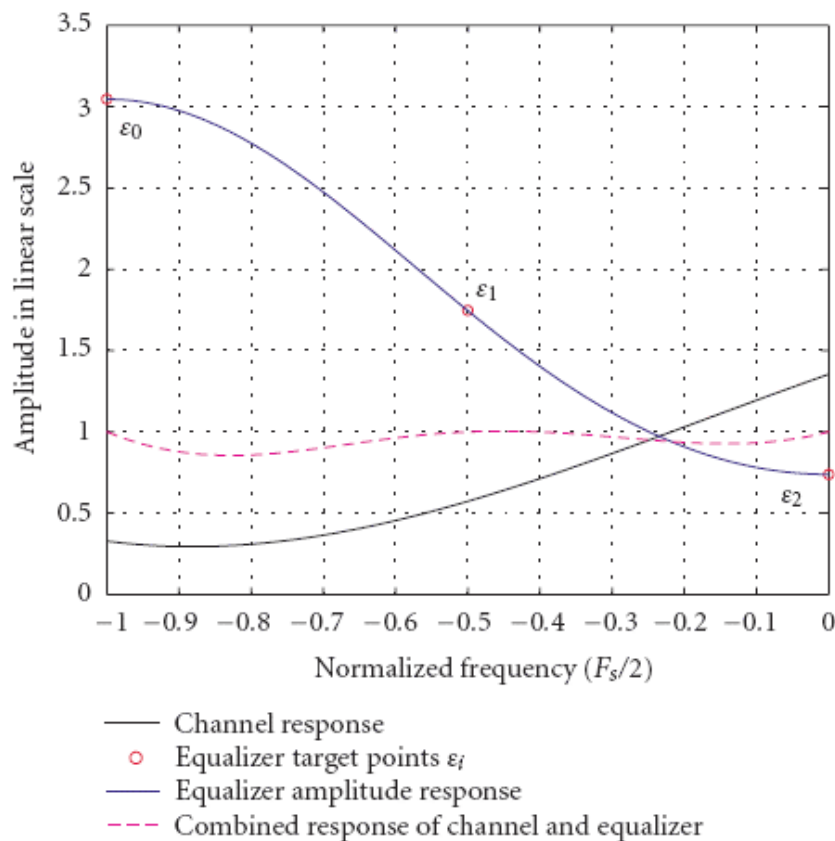


Figure 4-1-2. Illustration of frequency sampling based subchannel equalizer design.

The coefficients of a 1-tap, 2-tap, and 3-tap complex finite impulse response (FIR) filter-based subchannel equalizers (referred hereafter as Case 1, Case 2, and Case 3 structures, respectively) can be obtained through frequency-sampling design according to the following procedure. Let us assume that channel measurements at frequency grid with density twice compared to the number of subchannels in the analysis bank are available. In practice, these channel estimates can be obtained through 2-dimensional (over time-frequency plane) interpolation based on the channel estimates at the pilot positions. Channel estimates at the pilot positions can be obtained, e.g., with the Pairs of Pilots (POP) or Interference Approximation (IAM) approaches or using the auxiliary pilot –based estimation procedure (see Chapter 3 for details).

With the proposed filter bank structure, all subchannel signals alias around the zero-frequency, when down-sampled by $M/2$ in the analysis filter bank. Furthermore, let us denote the discrete set of target values of the subchannel equalizer response by $\chi_{k,i}$, $i \in \{0,1,2\}$ where subscript index $i=1$ corresponds to the subchannel center frequency whereas indexes $i=0$ and $i=2$ refer to the lower and the upper passband edge frequencies, respectively. The target values are calculated from the channel estimates at the corresponding frequency positions, denoted by $H_k^{(i)}$ (or by $H_{k,n}^{(i)}$ in case of time-variant channel), according to the zero-forcing (ZF) or the mean squared error (MSE) criterion.

With MSE criterion,

$$\chi_{k,i} = \mathcal{X}_{k,i}' ,$$

where

$$\mathcal{X}_{k,i}' = \frac{(H_k^{(i)})^*}{|H_k^{(i)}|^2 + \eta}$$

and

$$\gamma = \frac{3}{\sum_{i=0}^2 \mathcal{X}_{k,i}' H_k^{(i)}} .$$

Above, γ and η denote a scaling factor, which normalizes the subchannel signal power, and the noise-to-signal power ratio, respectively. Moreover, for the Case 2 structure, operating on two target frequency points, $\gamma = 2 / (\mathcal{X}_{k,0}' H_k^{(0)} + \mathcal{X}_{k,2}' H_k^{(2)})$. In case of the ZF criterion, $\eta = 0$ and $\gamma=1$.

The frequency-sampling design of the complex FIR filter-based subchannel equalizer proceeds as follows:

Case 3:

The transfer function of a 3-tap FIR (Case 3 structure) is expressed by

$$W_k(z) = w_{k,-1}z + w_{k,0} + w_{k,1}z^{-1} .$$

The frequency points corresponding to the frequency positions of the targets values, at the low rate after decimation, are $\left\{-\frac{\pi}{2}, 0, \frac{\pi}{2}\right\}$. By evaluating the transfer function $W_k(e^{j\omega})$ at these frequency points of interest and setting the resulting expressions equal to the corresponding target values $\chi_{k,i}$, the following set of equations can be derived

$$\begin{aligned} W_k\left(e^{-j\frac{\pi}{2}}\right) &= -jw_{k,-1} + w_{k,0} + jw_{k,1} = \chi_{k,0} \\ W_k\left(e^{j0}\right) &= w_{k,-1} + w_{k,0} + w_{k,1} = \chi_{k,1} \\ W_k\left(e^{j\frac{\pi}{2}}\right) &= jw_{k,-1} + w_{k,0} - jw_{k,1} = \chi_{k,2} . \end{aligned}$$

This set of three equations with three unknowns $\{w_{k,-1}, w_{k,0}, w_{k,1}\}$ can be easily solved and yields

$$\begin{aligned} w_{k,-1} &= \frac{-\chi_{k,0}(1-j) + 2\chi_{k,1} - \chi_{k,2}(1+j)}{4} \\ w_{k,0} &= \frac{\chi_{k,0} + \chi_{k,2}}{2} . \\ w_{k,1} &= \frac{-\chi_{k,0}(1+j) + 2\chi_{k,1} - \chi_{k,2}(1-j)}{4} \end{aligned}$$

Case 2:

The 2-tap complex FIR filter (Case 2 structure) can be derived in similar manner, bearing in mind that now only two frequency points, specifically those of the passband edge frequencies, are used in the design. Now the transfer function of the considered filter can be expressed as

$$W_k(z) = w_{k,0} + w_{k,1}z^{-1} .$$

The relevant frequency points at the low rate now become $\left\{-\frac{\pi}{2}, \frac{\pi}{2}\right\}$. By evaluating the transfer function $W_k(e^{j\omega})$ at these frequency points and setting the resulting expressions equal to the corresponding target values $\chi_{k,i}$, the following set of equations can be obtained

$$\begin{aligned} W_k\left(e^{-j\frac{\pi}{2}}\right) &= w_{k,0} + jw_{k,1} = \chi_{k,0} \\ W_k\left(e^{j\frac{\pi}{2}}\right) &= w_{k,0} - jw_{k,1} = \chi_{k,2} . \end{aligned}$$

This set of two equations can again be solved for the two unknowns $\{w_{k,0}, w_{k,1}\}$ and gives

$$\begin{aligned} w_{k,0} &= \frac{\chi_{k,0} + \chi_{k,2}}{2} , \\ w_{k,1} &= \frac{\chi_{k,0} - \chi_{k,2}}{2j} \end{aligned}$$

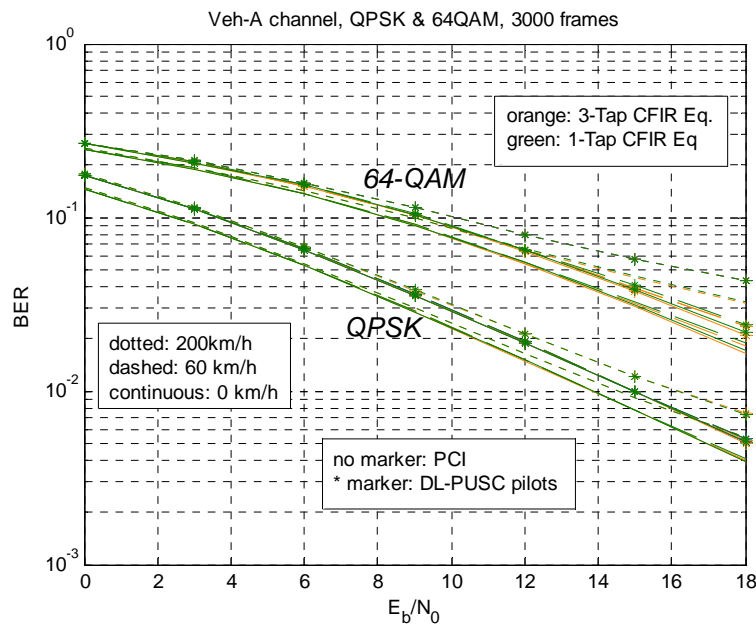
Case 1:

In this case the subchannel equalizer structure reduces to a single complex coefficient. Moreover, now only one frequency point per subchannel is used in the design. It is natural to select the inverse of the channel estimate at the subchannel center frequency as the target value, which then gives,

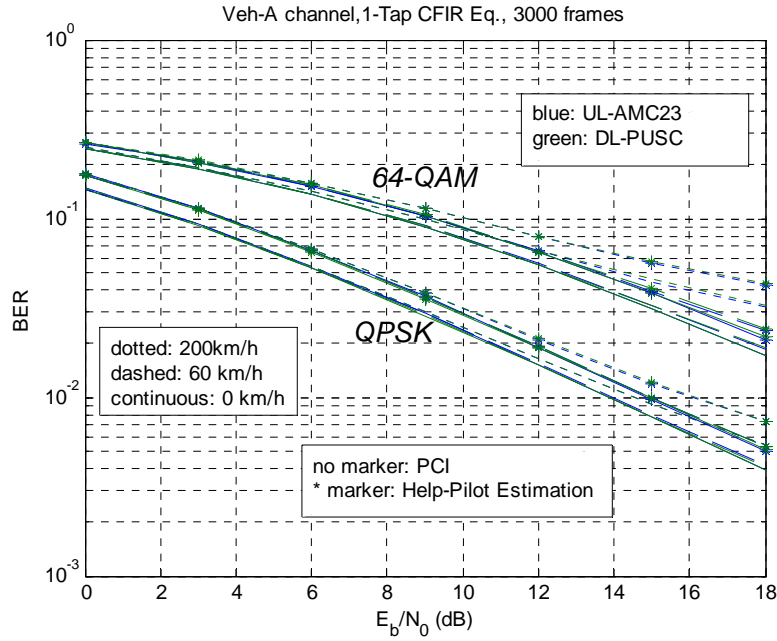
$$w_{k,0} = \chi_{k,1}.$$

Performance evaluation

- $M=1024$, M_u according to WiMAX profile
 - CNAM prototype, $K=4$
 - Veh-A Channel Model
 - Pilots according to WiMAX pilot profiles
 - 6 dB combined (pilot + help pilot) boost
 - Triangle-based linear interpolation between pilots (Delaunay triangulation, cf. Matlab `griddata` function)
- comparison between 1-tap and 3-tap equalizers



- effects of different WiMAX-like pilot schemes



4.2 Multiple taps equalizers

4.2.1 Fractionally spaced MMSE per-subcarrier equalizer

The subcarrier equalizers at the receiver are necessary in order to remove the intersymbol (ISI) and interchannel interference (ICI) in the subcarrier signals. Those are caused by the frequency selective Rayleigh fading channel since no redundancy in the sense of a guard interval like the CP is to be inserted.

We use only one FIR equalizer per subcarrier, i.e., only the output signal of the corresponding subcarrier at the receiver is used for the estimation of the transmit symbols in order to achieve a low complexity. The complexity is, therefore, linear in terms of the used subcarriers M_u and linear in terms of the equalizer coefficients L_{eq} .

Nevertheless, the $T/2$ spacing of the equalizer allows for practically removing the ICI of the adjacent subcarrier signals at the receiver. This means that the orthogonality of OQAM systems can be recovered again. The ICI of non-adjacent subcarriers is controlled by the high stopband attenuation of the subcarrier filters with roll-off $\alpha \leq 1$.

Because of the orthogonal multiplexing of the subcarrier signals, we have to modify the conventional MMSE equalization [21]. This equalization concept can also be used in OQAM single carrier systems in a very similar way to [22]. The crucial idea in the application of multicarrier systems is that the ICI of adjacent subcarriers can also be introduced in the optimization procedure. We, therefore, use the statistical information on the immediately adjacent subcarrier symbols in order to get a regularization term for the resulting Wiener-Hopf equation of the MSE minimization. Thus the interference is taken into account in the optimization process very similar to the noise.

Again, the high stopband attenuation allows for omitting information about further subcarriers for the sake of low complexity.

The orthogonal multiplexing of the filter bank prevents a straightforward derivation of the MMSE solution. The key in solving this optimization problem is to split the complex symbols and filter coefficients into real and imaginary parts. According to the characteristics of the OQAM-FBMC the role of the real and imaginary part operators is interchanged from subcarrier to subcarrier. This certainly holds true for the destaggering O_k^0 (Fig. 4-4-3).

The output $y_{k,n}$ of the AFB subcarrier filters is then filtered by the subcarrier equalizer $w_{k,n}$ of length L_{eq} . The resulting subcarrier signal is destaggered by O_k^0 , which downsamples the signal by two and gives the estimation $\tilde{d}_{k,n}$ by the real part and $\tilde{d}_{k,n}$ by j times the imaginary part as depicted in Fig. 4-4-3.

Our design criterion is to minimize the mean square error (MSE) between the estimated signal $\tilde{d}_{k,n}$ and the input signal $d_{k,n}$.

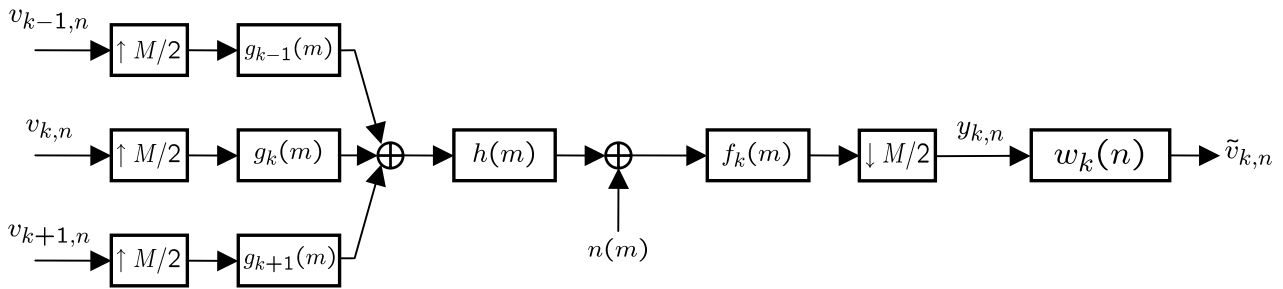


Figure 4-2-1. Subcarrier model for the FBMC system.

Based on the system model in Figure 4-2-1, we have⁴:

$$\mathbf{y}_{k,n} = \mathbf{Q}_{k,k-1} \mathbf{v}_{k-1,n} + \mathbf{Q}_{k,k} \mathbf{v}_{k,n} + \mathbf{Q}_{k,k+1} \mathbf{v}_{k+1,n} + \mathbf{\Gamma}_k \mathbf{n}(m) \quad (22)$$

where $\mathbf{y}_{i,n} = [y_{i,n}, \dots, y_{i,n-L_{eq}+1}]^T$ is an $L_{eq} \times 1$ column vector, $\mathbf{v}_{i,n} = [v_{i,n}, \dots, v_{i,n-N+1}]^T$ an $N \times 1$ column vector of OQAM symbols transmitted on the i -th subchannel and $\mathbf{Q}_{i,j}$ denotes an $L_{eq} \times N$ convolution matrix constructed from the cascade: $\uparrow M/2$, $g_i(m)$, $h(m)$, $f_j(m)$ and $\downarrow M/2$. $\mathbf{n}(m)$ is the $L + (L_{eq} - 1)M/2 \times 1$ additive white Gaussian noise vector. $\mathbf{\Gamma}_j$ is an $L_{eq} \times L + (L_{eq} - 1)M/2$ convolution matrix constructed from the cascade $f_j(m)$ and $\downarrow M/2$.

⁴ For more details about the derivation refer to [21], since the developments are quite similar.

In order to recover the transmitted symbols, the subchannel output $y_{k,n}$ is filtered by the equalizers $w_k(n)$. Let:

$$\bar{\mathbf{v}}_{k,n} = [\mathbf{v}_{k-1,n}^T \quad \mathbf{v}_{k,n}^T \quad \mathbf{v}_{k+1,n}^T]^T, \quad \text{and} \quad \mathbf{Q}_k = [\mathbf{Q}_{k,k-1} \quad \mathbf{Q}_{k,k} \quad \mathbf{Q}_{k,k+1}]$$

Subsequently, we have

$$\mathbf{y}_{k,n} = \mathbf{Q}_k \bar{\mathbf{v}}_{k,n} + \Gamma_k \mathbf{n}(m) \quad (23)$$

Now, the equalizer output can be written as:

$$\begin{aligned} \tilde{d}_{k,n} &= \text{Re}\{\mathbf{w}_k^H \mathbf{y}_{k,n}\} = \mathbf{w}_k^{(R),T} \mathbf{y}_{k,n}^{(R)} + \mathbf{w}_k^{(I),T} \mathbf{y}_{k,n}^{(I)}, \quad \text{for } k+n \text{ even} \\ \tilde{d}_{k,n} &= \text{Im}\{\mathbf{w}_k^H \mathbf{y}_{k,n}\} = \mathbf{w}_k^{(R),T} \mathbf{y}_{k,n}^{(I)} - \mathbf{w}_k^{(I),T} \mathbf{y}_{k,n}^{(R)}, \quad \text{for } k+n \text{ odd} \end{aligned} \quad (24)$$

$\mathbf{y}_{k,n}^{(R)}$ and $\mathbf{y}_{k,n}^{(I)}$ can be expressed as follows:

$$\begin{aligned} \mathbf{y}_{k,n}^{(R)} &= \overline{\mathbf{Q}}_k^{(R)} \bar{\mathbf{v}}_{k,n} + \text{Re}\{\Gamma_k \mathbf{n}(m)\} \\ \mathbf{y}_{k,n}^{(I)} &= \overline{\mathbf{Q}}_k^{(I)} \bar{\mathbf{v}}_{k,n} + \text{Im}\{\Gamma_k \mathbf{n}(m)\} \end{aligned} \quad (25)$$

where $\overline{\mathbf{Q}}_k^{(R)}$ and $\overline{\mathbf{Q}}_k^{(I)}$ are, respectively, the real and imaginary parts of $\overline{\mathbf{Q}}_k$. $\overline{\mathbf{Q}}_k$ and $\bar{\mathbf{v}}_{k,n}$ are obtained from \mathbf{Q}_k and $\bar{\mathbf{v}}_{k,n}$, respectively by shifting the complex number $j = \sqrt{-1}$ from the imaginary entries of $\bar{\mathbf{v}}_{k,n}$ into the corresponding columns of \mathbf{Q}_k . This is done before taking the real or imaginary parts. Finally, we get the compact expression:

$$\tilde{d}_{k,n} = \overline{\mathbf{w}}_k^T \bar{\mathbf{y}}_{k,n} \quad (26)$$

where $\bar{\mathbf{y}}_{k,n} = \begin{bmatrix} \mathbf{y}_{k,n}^{(R)} \\ \mathbf{y}_{k,n}^{(I)} \end{bmatrix}$ and $\overline{\mathbf{w}}_k = \begin{bmatrix} \mathbf{w}_k^{(R)} \\ \mathbf{w}_k^{(I)} \end{bmatrix}$.

In order to compute the equalizer coefficients, we propose to minimize a classical MMSE criterion. It is given by:

$$J = E[(\tilde{d}_{k,n} - d_{k,n-\nu})^2] = E[(\overline{\mathbf{w}}_k^T \bar{\mathbf{y}}_{k,n} - d_{k,n-\nu})^2] \quad (27)$$

where ν is the equalizer delay and can be chosen properly.

Now by differentiating (27) with respect to $\overline{\mathbf{w}}_k$ and setting it equal to zero, we can easily find the following expression:

$$\overline{\mathbf{w}}_k = [\overline{\mathbf{Q}}_k \mathbf{R}_{\bar{\mathbf{v}}} \overline{\mathbf{Q}}_k^T + \mathbf{R}_{\mathbf{n},k}]^{-1} \overline{\mathbf{Q}}_k \mathbf{R}_{\bar{\mathbf{v}}} \mathbf{e}_{N+\nu} \quad (28)$$

where $\overline{\mathbf{Q}}_k = \begin{bmatrix} \overline{\mathbf{Q}}_k^{(R)} \\ \overline{\mathbf{Q}}_k^{(I)} \end{bmatrix}$, $\mathbf{R}_{\bar{\mathbf{v}}} = E[\bar{\mathbf{v}}_{k,n} \bar{\mathbf{v}}_{k,n}^T] = \sigma_d^2 I_{3N}$, $\mathbf{e}_{N+\nu}$ is the null vector with 1 in its $N+\nu$ entry and $\mathbf{R}_{\mathbf{n},k} = \begin{bmatrix} \mathbf{R}'_{\mathbf{n},k} & \mathbf{R}''_{\mathbf{n},k} \\ -\mathbf{R}''_{\mathbf{n},k} & \mathbf{R}'_{\mathbf{n},k} \end{bmatrix}$, with :

$$\begin{aligned} \mathbf{R}'_{\mathbf{n},k} &= 0.5 \left(\Gamma_k^{(R)} \mathbf{R}_{\mathbf{n}} \Gamma_k^{(R),T} + \Gamma_k^{(I)} \mathbf{R}_{\mathbf{n}} \Gamma_k^{(I),T} \right) \\ \mathbf{R}''_{\mathbf{n},k} &= 0.5 \left(\Gamma_k^{(R)} \mathbf{R}_{\mathbf{n}} \Gamma_k^{(I),T} - \Gamma_k^{(I)} \mathbf{R}_{\mathbf{n}} \Gamma_k^{(R),T} \right) \end{aligned}$$

and $\mathbf{R}_{\mathbf{n}} = E[\mathbf{n}(m)\mathbf{n}(m)^T] = \sigma_n^2 \mathbf{I}$ for uncorrelated stationary noise, where σ_n^2 is the noise power.

Eventually, \mathbf{w}_k can be easily recovered from $\bar{\mathbf{w}}_k$.

With the steps from above we have found the analytical solution for the L_{eq} -tap FIR equalizer yielding the MMSE. This solution can also be approached in an adaptive way we will see in Section 4.4.

4.2.2 Simplified MMSE equalizer

In this section, we propose a simplified version of the MMSE equalizer presented in the previous section. The idea here is to consider only the subchannel of interest instead of considering the adjacent subchannels at the transmitter to model the system as in Section 4.2.1, whence the name simplified MMSE equalizer. This model does not take into account the interference of the adjacent subchannels, but as we will see in simulations, in the case of short transmission channels, the equalizer based on this model performs almost like the MMSE in Section 4.2.1. Figure 4-2-2 shows the simplified model used in the computation of the simplified MMSE equalizer.

In terms of mathematical description of the equalizer, the equation is similar to the one in (28), but only the term corresponding to the adjacent subchannels at the transmitter is removed. This corresponds to take in (23):

$$\bar{\mathbf{v}}_{k,n} = \mathbf{v}_{k,n}, \quad \text{and} \quad \mathbf{Q}_k = \mathbf{Q}_{k,k}$$

Remark: Note that the performance of these two equalizers will be presented in Section 4.3, in comparison with the multiple band MMSE equalizer.

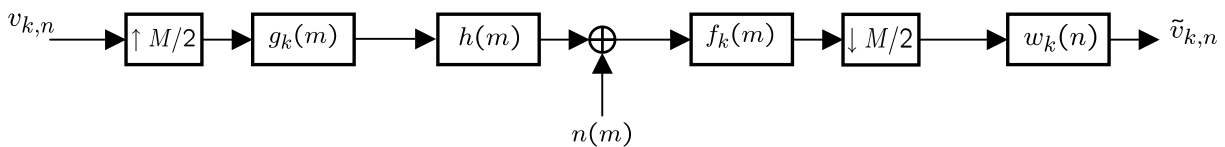


Figure 4-2-2. System model for the simplified MMSE equalizer.

4.3 Multiple band MMSE equalizer

In the MMSE equalizer and simplified MMSE, only the subchannel output of interest is used for computing the equalizer. In this section, we will also use the output of the immediate adjacent subchannels in order to further improve the equalizer performance. We refer to the corresponding equalizer by multiple band MMSE equalizer. The considered system model is depicted in Figure 4-3-1.

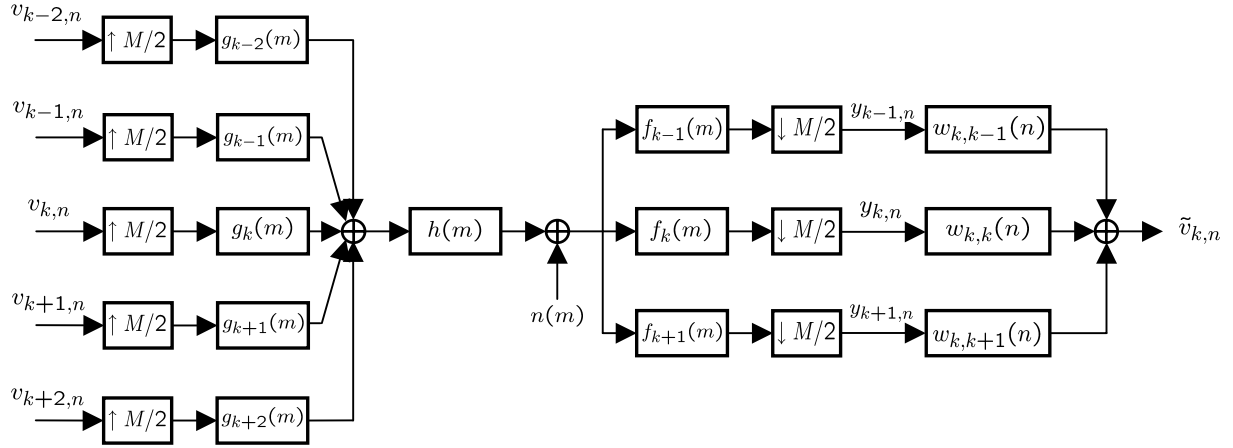


Figure 4-3-1. System model for the multiple band MMSE equalizer.

Based on the system model in Figure 4-3-1, we have⁵:

$$\begin{aligned} \mathbf{y}_{k-1,n} &= \mathbf{Q}_{k-1,k-2} \mathbf{v}_{k-2,n} + \mathbf{Q}_{k-1,k-1} \mathbf{v}_{k-1,n} + \mathbf{Q}_{k-1,k} \mathbf{v}_{k,n} + \mathbf{\Gamma}_{k-1} \mathbf{n}(m) \\ \mathbf{y}_{k,n} &= \mathbf{Q}_{k,k-1} \mathbf{v}_{k-1,n} + \mathbf{Q}_{k,k} \mathbf{v}_{k,n} + \mathbf{Q}_{k,k+1} \mathbf{v}_{k+1,n} + \mathbf{\Gamma}_k \mathbf{n}(m) \\ \mathbf{y}_{k+1,n} &= \mathbf{Q}_{k+1,k} \mathbf{v}_{k,n} + \mathbf{Q}_{k+1,k+1} \mathbf{v}_{k+1,n} + \mathbf{Q}_{k+1,k+2} \mathbf{v}_{k+2,n} + \mathbf{\Gamma}_{k+1} \mathbf{n}(m) \end{aligned} \quad (29)$$

where $\mathbf{y}_{i,n} = [y_{i,n}, \dots, y_{i,n-L_{eq}+1}]^T$ is an $L_{eq} \times 1$ column vector, $\mathbf{v}_{i,n} = [v_{i,n}, \dots, v_{i,n-N+1}]^T$ an $N \times 1$ column vector of OQAM symbols transmitted on the i -th subchannel and $\mathbf{Q}_{i,j}$ denotes an $L_{eq} \times N$ convolution matrix constructed from the cascade: $\uparrow M/2$, $g_i(m)$, $h(m)$, $f_j(m)$ and $\downarrow M/2$. $\mathbf{n}(m)$ is the $L + (L_{eq} - 1)M/2 \times 1$ additive white Gaussian noise vector. $\mathbf{\Gamma}_j$ is an $L_{eq} \times L + (L_{eq} - 1)M/2$ convolution matrix constructed from the cascade $f_j(m)$ and $\downarrow M/2$.

In order to recover the transmitted symbols, the subchannels outputs $y_{k-1,n}$, $y_{k,n}$ and $y_{k+1,n}$ are filtered by the equalizers $w_{k,k-1}(n)$, $w_{k,k}(n)$, and $w_{k,k+1}(n)$, respectively. Let:

⁵ For more details about the derivation refer to [21], since the developments are quite similar.

$$\bar{\mathbf{y}}_{k,n} = \begin{bmatrix} \mathbf{y}_{k-1,n} \\ \mathbf{y}_{k,n} \\ \mathbf{y}_{k+1,n} \end{bmatrix}, \bar{\mathbf{v}}_{k,n} = [\mathbf{v}_{k-2,n}^T \quad \mathbf{v}_{k-1,n}^T \quad \mathbf{v}_{k,n}^T \quad \mathbf{v}_{k+1,n}^T \quad \mathbf{v}_{k+2,n}^T]^T, \quad \bar{\mathbf{\Gamma}}_{k-1} = \begin{bmatrix} \mathbf{\Gamma}_{k-1} \\ \mathbf{\Gamma}_k \\ \mathbf{\Gamma}_{k+1} \end{bmatrix}, \text{ and}$$

$$\mathbf{Q}_k = \begin{bmatrix} \mathbf{Q}_{k-1,k-2} & \mathbf{Q}_{k-1,k-1} & \mathbf{Q}_{k-1,k} & \mathbf{0} & \mathbf{0} \\ \mathbf{0} & \mathbf{Q}_{k,k-1} & \mathbf{Q}_{k,k} & \mathbf{Q}_{k,k+1} & \mathbf{0} \\ \mathbf{0} & \mathbf{0} & \mathbf{Q}_{k+1,k} & \mathbf{Q}_{k+1,k+1} & \mathbf{Q}_{k+1,k+2} \end{bmatrix}$$

Subsequently, we have

$$\bar{\mathbf{y}}_{k,n} = \mathbf{Q}_k \bar{\mathbf{v}}_{k,n} + \bar{\mathbf{\Gamma}}_k \mathbf{n}(m) \quad (30)$$

and let $\bar{\mathbf{w}}_k = [\mathbf{w}_{k,k-1}^T \quad \mathbf{w}_{k,k}^T \quad \mathbf{w}_{k,k+1}^T]^T$. Note that we consider here the same equalizer length L_{eq} for $\mathbf{w}_{k,k-1}^T$, $\mathbf{w}_{k,k}^T$ and $\mathbf{w}_{k,k+1}^T$, but it could be chosen differently. Now, the equalizer output can be written as:

$$\begin{aligned} \tilde{d}_{k,n} &= \text{Re}\{\bar{\mathbf{w}}_k^H \bar{\mathbf{y}}_{k,n}\} = \bar{\mathbf{w}}_k^{(R),T} \bar{\mathbf{y}}_{k,n}^{(R)} + \bar{\mathbf{w}}_k^{(I),T} \bar{\mathbf{y}}_{k,n}^{(I)}, \text{ for } k+n \text{ even} \\ \tilde{d}_{k,n} &= \text{Im}\{\bar{\mathbf{w}}_k^H \bar{\mathbf{y}}_{k,n}\} = \bar{\mathbf{w}}_k^{(R),T} \bar{\mathbf{y}}_{k,n}^{(I)} - \bar{\mathbf{w}}_k^{(I),T} \bar{\mathbf{y}}_{k,n}^{(R)}, \text{ for } k+n \text{ odd} \end{aligned} \quad (31)$$

$\bar{\mathbf{y}}_{k,n}^{(R)}$ and $\bar{\mathbf{y}}_{k,n}^{(I)}$ can be expressed as follows:

$$\begin{aligned} \bar{\mathbf{y}}_{k,n}^{(R)} &= \bar{\mathbf{Q}}_k^{(R)} \bar{\mathbf{v}}_{k,n} + \text{Re}\{\bar{\mathbf{\Gamma}}_k \mathbf{n}(m)\} \\ \bar{\mathbf{y}}_{k,n}^{(I)} &= \bar{\mathbf{Q}}_k^{(I)} \bar{\mathbf{v}}_{k,n} + \text{Im}\{\bar{\mathbf{\Gamma}}_k \mathbf{n}(m)\} \end{aligned} \quad (32)$$

where $\bar{\mathbf{Q}}_k^{(R)}$ and $\bar{\mathbf{Q}}_k^{(I)}$ are, respectively, the real and imaginary parts of $\bar{\mathbf{Q}}_k$. $\bar{\mathbf{Q}}_k$ and $\bar{\mathbf{v}}_{k,n}$ are obtained from \mathbf{Q}_k and $\bar{\mathbf{v}}_{k,n}$, respectively by shifting the complex number $j = \sqrt{-1}$ from the imaginary entries of $\bar{\mathbf{v}}_{k,n}$ into the corresponding columns of \mathbf{Q}_k . This is done before taking the real or imaginary parts. Finally, we get the compact expression:

$$\tilde{d}_{k,n} = \bar{\mathbf{w}}_k^T \bar{\mathbf{y}}_{k,n} \quad (33)$$

where $\bar{\mathbf{y}}_{k,n} = \begin{bmatrix} \bar{\mathbf{y}}_{k,n}^{(R)} \\ \bar{\mathbf{y}}_{k,n}^{(I)} \end{bmatrix}$ and $\bar{\mathbf{w}}_k = \begin{bmatrix} \bar{\mathbf{w}}_k^{(R)} \\ \bar{\mathbf{w}}_k^{(I)} \end{bmatrix}$.

In order to compute the equalizer coefficients, we propose to minimize a classical MSE cost. It is given by:

$$J = E[(\tilde{d}_{k,n} - d_{k,n-\nu})^2] = E[(\bar{\mathbf{w}}_k^T \bar{\mathbf{y}}_{k,n} - d_{k,n-\nu})^2] \quad (34)$$

where ν is the equalizer delay and can be chosen properly.

Now by differentiating (34) with respect to $\bar{\mathbf{w}}_k$ and setting it equal to zero, we can easily arrive at the following expression:

$$\bar{\mathbf{w}}_k = [\bar{\mathbf{Q}}_k \mathbf{R}_{\bar{\mathbf{v}}} \bar{\mathbf{Q}}_k^T + \mathbf{R}_{\mathbf{n},k}]^{-1} \bar{\mathbf{Q}}_k \mathbf{R}_{\bar{\mathbf{v}}} \mathbf{e}_{N+\nu} \quad (35)$$

where $\bar{\mathbf{Q}}_k = \begin{bmatrix} \bar{\mathbf{Q}}_k^{(R)} \\ \bar{\mathbf{Q}}_k^{(I)} \end{bmatrix}$, $\mathbf{R}_{\bar{\mathbf{v}}} = E[\bar{\mathbf{v}}_{k,n} \bar{\mathbf{v}}_{k,n}^T] = \sigma_d^2 I_{3N}$, $\mathbf{e}_{N+\nu}$ is the null vector with 1 in its $N+\nu$ entry and

$$\mathbf{R}_{\mathbf{n},k} = \begin{bmatrix} \mathbf{R}'_{\mathbf{n},k} & \mathbf{R}''_{\mathbf{n},k} \\ -\mathbf{R}''_{\mathbf{n},k} & \mathbf{R}'_{\mathbf{n},k} \end{bmatrix}, \text{ with :}$$

$$\mathbf{R}'_{\mathbf{n},k} = 0.5(\bar{\Gamma}_k^{(R)} \mathbf{R}_{\mathbf{n}} \bar{\Gamma}_k^{(R),T} + \bar{\Gamma}_k^{(I)} \mathbf{R}_{\mathbf{n}} \bar{\Gamma}_k^{(I),T})$$

$$\mathbf{R}''_{\mathbf{n},k} = 0.5(\bar{\Gamma}_k^{(R)} \mathbf{R}_{\mathbf{n}} \bar{\Gamma}_k^{(I),T} - \bar{\Gamma}_k^{(I)} \mathbf{R}_{\mathbf{n}} \bar{\Gamma}_k^{(R),T})$$

and $\mathbf{R}_{\mathbf{n}} = E[\mathbf{n}(m)\mathbf{n}(m)^T] = \sigma_n^2 \mathbf{I}$ for uncorrelated stationary noise.

Eventually, $\mathbf{w}_{k,k-1}^T$, $\mathbf{w}_{k,k}^T$ and $\mathbf{w}_{k,k+1}^T$ can be easily recovered from $\bar{\mathbf{w}}_k$.

Numerical results:

In order to assess the performance of these two equalizers, we consider the following simulation parameters: $M=M_u=64$ or 256 , $K=4$, $L=KM$, $f_s=11.2 \text{ MHz}$, 16-QAM modulation, PHYDYAS reference filter bank, and Veh-A channel. In all simulations, the channel is assumed to be perfectly estimated. Note that WiMAX parameters will be considered in Section 5.

Figure 4-3-2 compares the multiple band MMSE and simplified MMSE equalizers with the MMSE equalizer and the classical one tap equalizer. Figure 4-3-2 plots the performance in terms of bit error rate (BER) versus E_b/N_0 . We have considered $M=64$, thus in this case the channel is highly selective. In order to be more objective in comparing the algorithms, we have chosen the same equalizer length, 3, for equalizers MMSE and simplified MMSE. For the multiple band MMSE equalizer, the equalizer length for the subchannel of interest is 3 and 1 for each adjacent subchannel. These equalizers lengths are considered in all simulations. We observe that the MMSE and multiple band MMSE are better than the others and the performance of both of them is almost the same. Based on these results, it is clear that the MMSE equalizer, in this case, represents the best performance/complexity tradeoff. Note that in this case the simplified MMSE equalizer is not attractive.

In Figure 4-3-3, we have considered the same parameters as in Figure 4-3-2 but with $M=256$. In this case, the channel is much shorter than the FBMC symbol. Figure 4-3-3 shows that the MMSE, multiple band MMSE and simplified MMSE have almost the same performance for low SNR. However, the MMSE and multiple band MMSE outperform the simplified MMSE and the classical one tap equalizer for high SNR. In this case, the simplified MMSE presents an acceptable performance with lower complexity compared to the MMSE.

Based on these results, we can say that, firstly, the MMSE is the best equalizer, and secondly the multiple band MMSE performs almost like MMSE but with higher complexity. Therefore, it is not of particular interest in our case.

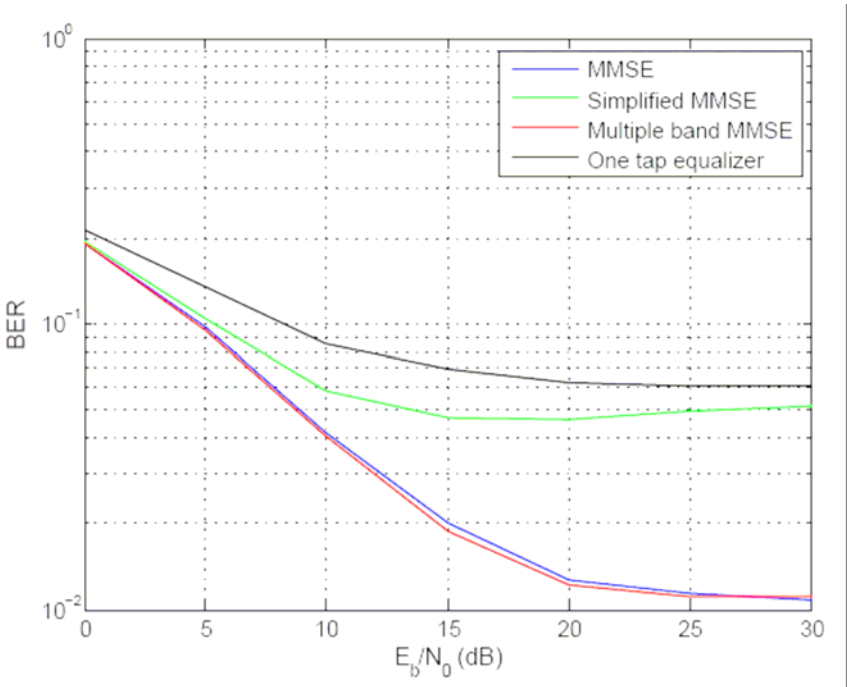


Figure 4-3-2. Comparison of different equalizers. BER versus E_b/N₀. M=64 and Veh-A channel.

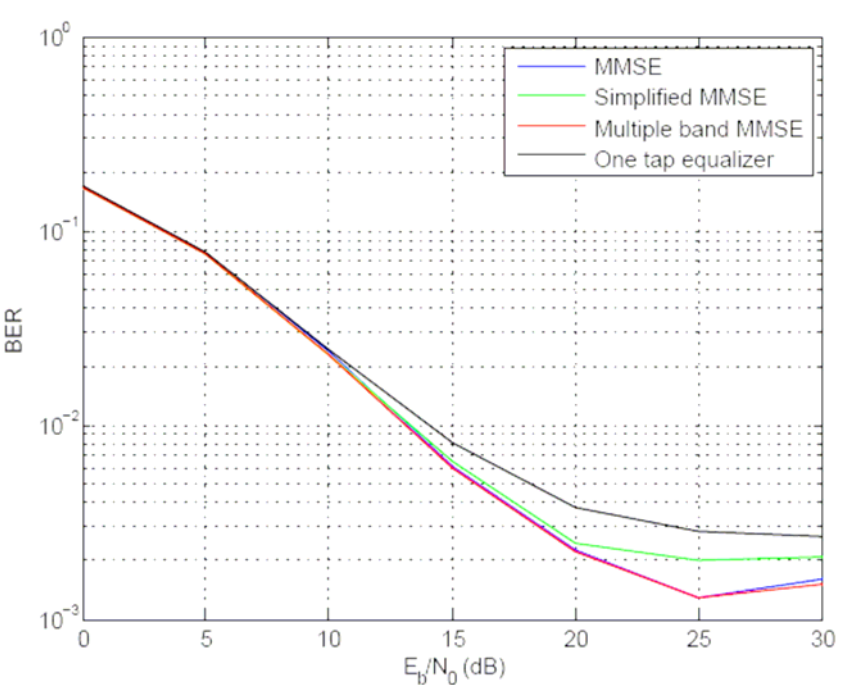


Figure 4-3-3. Comparison of different equalizers. BER versus E_b/N₀. M=256 and Veh-A channel.

4.4 Fractionally-spaced adaptive (LMS) per-subcarrier equalization

In this approach, the LMS algorithm is used as adaptive equalizer solution, aiming at the minimum mean-square error (MMSE). In the following, an adaptation of the LMS algorithm of QAM systems to the OQAM characteristics of the FBMC system is presented. Still a per-subcarrier equalizer which works at $T/2$, where T is the symbol duration, is used. The initial value of the LMS equalizer is obtained by a pilot-based channel estimation technique and interpolation between the frequency samples.

One FIR equalizer per subcarrier is employed to compensate for the intersymbol (ISI) and interchannel interference (ICI) caused by the frequency selective radio channel and improve the symbol decisions.

The complexity of the equalizer which is derived in this paper is limited by the fact that only directly adjacent subcarriers show significant overlap. We only use a single but $T/2$ -spaced equalizer for each subcarrier k of the M_u subcarriers (cf. Fig. 4-4-1), which are obtained by the exponential modulation of a zero-phase prototype filter $p[m]$ with length L according to

$$g_k[m] = p[m] e^{j \frac{2\pi k}{M} \left(m - \frac{L-1}{2} \right)}.$$

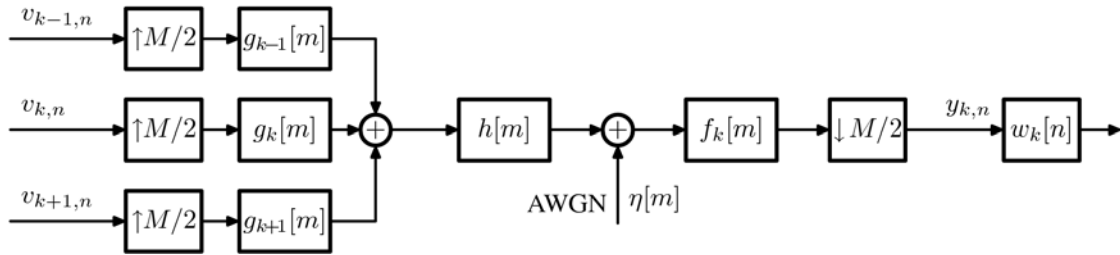


Fig. 4-4-1. Subcarrier model for the FBMC system.

Therefore, the equalizer is able to remove the distortion before aliasing of the spectral components occurs and allows for restoring the orthogonality of the subcarriers without considering the received symbols of adjacent carriers.

The conventional LMS algorithm [24] has to be adapted to the orthogonal multiplexing of the subcarriers [23]. After equalizing the received subcarrier signal $y_{k,n}$ with the LMS controlled FIR filter $\mathbf{w}_k[n]$, we get the following two equations for the estimation of the real and imaginary part of the input symbol according to Fig. 4-4-3:

$$\Re[\mathbf{w}_k^H[n] \mathbf{y}_{k,n}] = \mathbf{w}_k^{R,T}[n] \mathbf{y}_{k,n}^R + \mathbf{w}_k^{I,T}[n] \mathbf{y}_{k,n}^I = \tilde{d}_{k,n}, \quad \text{for } k+n \text{ even}, \quad (36)$$

$$\Im[\mathbf{w}_k^H[n] \mathbf{y}_{k,n}] = \mathbf{w}_k^{R,T}[n] \mathbf{y}_{k,n}^I - \mathbf{w}_k^{I,T}[n] \mathbf{y}_{k,n}^R = \tilde{d}_{k,n}, \quad \text{for } k+n \text{ odd}, \quad (37)$$

where $\mathbf{w}_k[n]$ and $\mathbf{y}_{k,n}$ are vectors, i.e. L_{eq} corresponds to the number of equalizer coefficients. $\tilde{d}_{k,n}$ is an estimate for the transmitted symbol $d_{k,n}$ of Fig. 4-4-2.

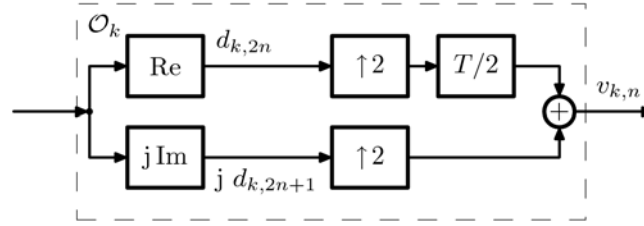


Fig. 4-4-2. OQAM staggering, k even

It is also important to mention that the OQAM structure necessitates that the real and imaginary parts of Figures. 4-4-3 and 4-4-2 be interchanged from subcarrier to subcarrier.

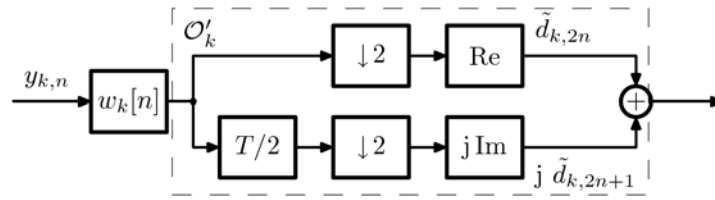


Fig. 4-4-3. OQAM destaggering, k even.

We use the same filter vector $\mathbf{w}_k[n]$ in (36) and (37) because it is optimum for both the real and imaginary part of $x_{k,n}$ under the assumption of additive white Gaussian noise and uncorrelated input symbols.

For updating the filter vector \mathbf{w}_k , we have to determine the error signal $\xi_{k,l}$ in Fig. 4-4-4 by

$$\xi_{k,2n} = \hat{d}_{k,2n} + j\hat{d}_{k,2n+1} - \tilde{d}_{k,2n} - j\tilde{d}_{k,2n+1} = Q[\tilde{d}_{k,2n} + j\tilde{d}_{k,2n+1}] - \tilde{d}_{k,2n} - j\tilde{d}_{k,2n+1},$$

where $Q[\tilde{d}_{k,2n} + j\tilde{d}_{k,2n+1}]$ determines the nearest symbol of the corresponding modulation alphabet from $\tilde{d}_{k,l}$ by a hard decision.

Therefore, we are able to update the filter vector every half symbol duration $T/2$, with either a pure real or a pure imaginary error signal. The error signal $e_{k,n}$ for the update process of the $T/2$ spaced filter vector results in

$$e_{k,n} = \begin{cases} \xi_{k,2n}^R, & n \in Z, \\ j\xi_{k,2n+1}^I, & n \in Z, \end{cases} \quad (38)$$

where the role of real and imaginary parts is interchanged again from subcarrier to subcarrier. In the QAM case, we would update only every symbol duration T but with complex instead of pure real or pure imaginary values.

The LMS adaptation is operated in the decision directed mode because the error is calculated based on the decisions of the estimated symbols $\tilde{d}_{k,n}$. It is clear that either a good initial value $\mathbf{w}_k[0]$ for the equalizer has to be provided or pilot symbols have to be sent. Otherwise the decision of the

symbols would be very unreliable and no convergence of the stochastic gradient based LMS algorithm would be achieved.

In the simulations, we will show how reasonable initial values $\mathbf{w}_k[0]$ are yielded by pilot based channel estimation, which allow for an operation in the decision directed mode.

The tap weight adaptation for the equalizer uses the error signal from (38) in the following way (cf. Fig. 4-4-4.):

$$\mathbf{w}_k[n+1] = \mathbf{w}_k[n] + \Delta \mathbf{w}_k[n] = \mathbf{w}_k[n] + \mu \mathbf{y}_{k,n} e_{k,n}^*,$$

where μ is the step-size parameter of the LMS algorithm.

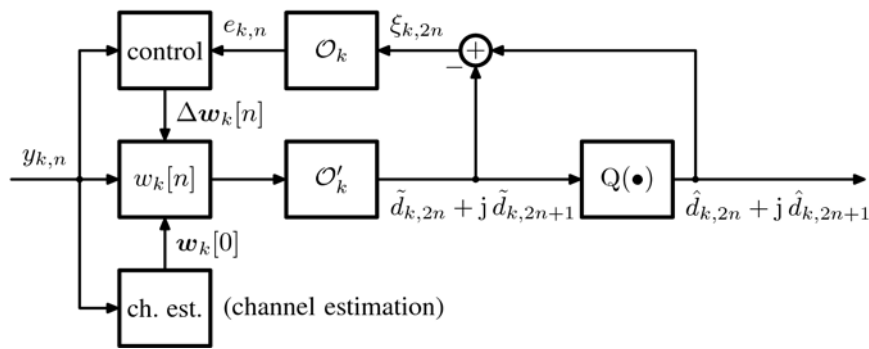


Figure 4-4-4. OQAM-LMS (Decision Directed Mode).

According to the literature [24], the step-size parameter μ can be chosen in relation to the correlation matrix \mathbf{R}_{y_k} of the equalizer input signal $\mathbf{y}_{k,n}$ or in an adaptive way as step-size for a normalized least means squares (NLMS) algorithm obtained by set-membership filtering theory. It is worth mentioning that this modified LMS algorithm can also be applied to single carrier systems with OQAM modulation.

In [23], some simulations for the LMS equalizer are shown in the context of HIPERLAN/2, where the channel estimate is obtained using CP-OFDM. Some changes have to be incorporated in the algorithm presented here to consider the channel estimation schemes in the context of WiMAX as presented in Section 3 of this document. Therefore, the results for the LMS equalizer using different channel estimation schemes will come in a later deliverable.

4.5 CFO compensation

Possible significant carrier frequency offset (CFO) would destroy the orthogonality of the subcarriers and degrade the system performance. The basic CFO compensation schemes are obviously the following (here ε is the carrier frequency offset normalized to subcarrier spacing):

- Time-domain compensation by multiplying the received signal with the complex-exponential sequence $e^{-j2\pi\varepsilon m/M}$.
- Frequency-domain compensation by multiplying the complex subcarrier signals by the complex-exponential sequence $e^{-j2\pi\varepsilon m/2}$.

Naturally, significant CFO must be compensated in time domain, but small values of offset can also be compensated in frequency domain. If the CFO estimation is done in time-domain, before the analysis filter bank, then it is straightforward to also compensate it in time-domain before the analysis filter bank. However, as discussed in Section 3-2 of PHYDYAS deliverable 2.1 [9], in the context of dynamical spectrum use, there are various advantages if the CFO and timing estimation functions can be moved to frequency domain [20]. Then frequency-domain estimates can be used straightforwardly in time-domain compensation during the next transmission burst. This is possible also for the next received symbol interval, through multiplying the contents of the polyphase branches of the analysis filter bank by the complex exponential sequence. However, if the detected CFO is too big for proper detection, re-iteration of the analysis filter bank is the only possibility, if the symbols which are used for CFO estimation contain also data. Occasional re-iteration of the analysis bank (e.g., during initialization) is not out of the question, even though it temporarily increases the processing load.

In a WiMAX-like system, after initial synchronization, only small CFO drift needs to be tracked and compensated, and there are no problems in using frequency-domain compensation. Whether frequency-domain processing is feasible also during the initialization phase is one interesting theme to be investigated.

Performance evaluation of frequency-domain CFO compensation

Figure 4-5-1 shows the performance of joint frequency-domain CFO compensation and channel equalization with 1-tap subcarrier equalizers for 64-QAM with Vehicular-A channel model. The E_b/N_0 -ratio is 20 dB. Three cases are shown:

- With perfect knowledge of CFO and channel.
- Auxiliary pilot based channel estimation and CFO estimation as described in [9]
- Auxiliary pilot based channel estimation and subcarrier equalization only (no explicit CFO compensation).

It can be observed that with 64-QAM, CFOs up to about $0.025 \Delta f$ can be compensated in frequency domain with good performance. CFO estimation quality is very good, and the degradation is due to imperfect channel estimation. Pilot-based channel estimation and equalization is able to compensate the CFO in this range rather well without any explicit CFO estimation.

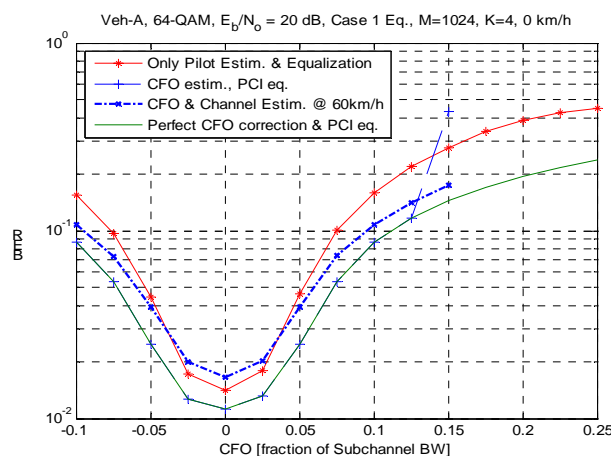


Figure 4-5-1. Frequency-domain CFO compensation performance for 64-QAM using 1-tap subcarrier equalizers and Veh-A channel model. $E_b/N_0=20$ dB.

4.6 Timing compensation

Similar to CFO, also timing offset estimation and compensation functions can be implemented in time or frequency domains. The time-domain compensation is easy to implement by adjusting the sampling phases in which the input samples are connected to the polyphase branches. If this needs to be done during a transmission frame, the contents of the polyphase branches can be re-organized in order to achieve instantaneous change in the timing between symbol intervals.

In frequency domain, the effect of timing offset is a linearly frequency-dependent phase response. Frequency-domain compensation of timing offset can be implemented in two different ways:

- Equalizing the phase response using sufficiently long subcarrier equalizers.
- Using fractional-delay filters to adjust the timing of the subcarrier signals in a proper way.

4.6.1 Performance evaluation of frequency-domain timing offset compensation using subcarrier equalizers

Figure 4-6-1 shows the performance of 1-tap and 3-tap subcarrier equalizers in compensating the timing offset with 4-QAM and 64-QAM modulations and Vehicular-A channel model. We can see that 1-tap equalizer gives sufficient performance with modest timing offsets only in case of low-order modulations. With 64-QAM, a multi-tap equalizer is needed if any timing offset is expected. The three-tap equalizer is sufficient for 4-QAM with practically any fractional time delay and for 64-QAM up to timing offsets of about 0.05T, i.e., about 50 samples.

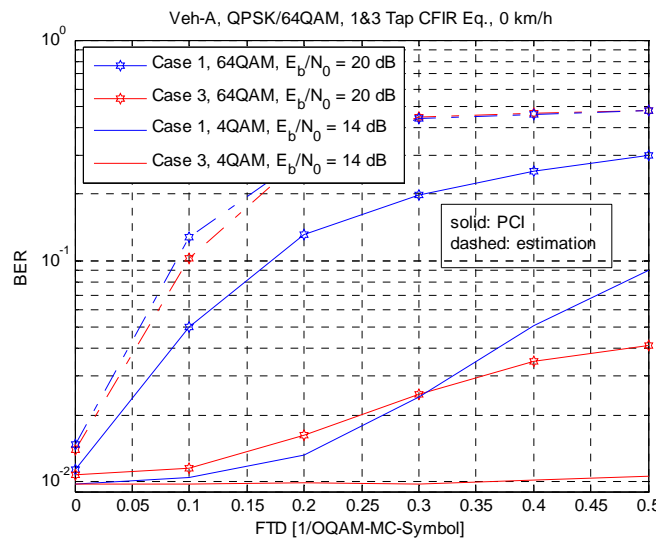


Figure 4-6-1. Frequency-domain timing offset compensation performance for 4-QAM and 64-QAM using 1 and 3-tap subcarrier equalizers with Veh-A channel model.

4.6.2 Interference minimization approach to timing offset compensation

As mentioned, the 3-tap channel equalizer can correct modest residual timing offsets even with high-order modulations. However, the timing offset estimation in frequency-domain using pilots is still a problem. One basic approach is to estimate the phase slope over the used signal band based on the phase of the subcarrierwise channel coefficients estimated using pilots. We have tested this idea using the auxiliary pilot approach, but the results (indicated also in Figure 4-6-1) are not encouraging. The problem is that timing offsets destroy the orthogonality of subcarriers and, consequently, the quality of pilots is degraded in the auxiliary pilot approach. It remains as a topic for future studies to test this approach using the paired-pilot approach.

Here we consider a completely different approach, which is jointly estimating the subcarrierwise channel coefficients and the phase slope. This approach utilizes the frequency selectivity introduced by the linear phase slope within each pilot subcarrier. We assume a simplified signal model, where the amplitude response is assumed to be constant within each subcarrier and the phase is assumed to be a linear function of frequency. This is motivated by the observation that 1-tap equalizer is able to equalize the channel quite well in the absence of timing offsets. The channel estimation includes two parts: estimation of the complex channel coefficient for each subcarrier, and estimation of the phase slope jointly for all used subcarriers.

If τ is the fractional time delay, expressed as a fraction of OQAM symbol interval T , and w_k is the 1-tap equalizer for subcarrier k in absence of timing offset, then the target response of the subcarrier equalizer in the frequency sampling design of Section 4.1.2 can be written as

$$\begin{aligned} W_k \left(e^{-j\frac{\pi}{2}} \right) &= w_k e^{j\psi} \\ W_k \left(e^{j0} \right) &= w_k \\ W_k \left(e^{j\frac{\pi}{2}} \right) &= w_k e^{-j\psi}, \end{aligned}$$

where

$$\psi = -\frac{\pi}{2} \frac{\tau}{T}$$

The subcarrier equalizer impulse response in the frequency sampling design can now be written as:

$$W_k(z) = \left[0.5(1 - \cos(\psi) - \sin(\psi))z + \cos(\psi) + 0.5(1 - \cos(\psi) + \sin(\psi))z^{-1} \right] w_k$$

We obtain the following signal model for the subcarrier equalizer output:

$$\begin{aligned} \tilde{y}_{k,n}(\psi) &= \cos(\psi)w_k y_{k,n} + 0.5(1 - \cos(\psi) + \sin(\psi))w_k y_{k,n-1} + 0.5(1 - \cos(\psi) - \sin(\psi))w_k y_{k,n+1} \\ &\approx w_k y_{k,n} + \frac{\psi}{2} w_k (y_{k,n-1} - y_{k,n+1}) \end{aligned}$$

This can be written as:

$$\begin{aligned}
\tilde{d}_{k,n} + j\tilde{u}_{k,n} &= \theta^{-(k+n)} \tilde{y}_{k,n}(\psi) = \theta^{-(k+n)} \left(w_k y_{k,n} + \frac{\psi}{2} w_k (y_{k,n-1} - y_{k,n+1}) \right) \\
&= w_k \theta^{-(k+n)} y_{k,n} + \frac{\psi}{2} w_k \theta^{-(k+n)} (y_{k,n-1} - y_{k,n+1}) \\
&= w_k z_{k,n} + \psi w_k \bar{z}_{k,n}
\end{aligned}$$

where

$$\begin{aligned}
z_{k,n} &= \theta^{-(k+n)} y_{k,n} \\
\bar{z}_{k,n} &= \theta^{-(k+n)} (y_{k,n-1} - y_{k,n+1}) / 2
\end{aligned}$$

Using the auxiliary pilot scheme, for the pilot symbols the ideal output is $d_{k,n}$. Now, the channel equalization problem can be formulated as:

$$\{\hat{\psi}, \hat{w}_k\} = \arg \min_{\psi, w_k} \left\{ \sum_{k,n \in \Omega_{TO}} |d_{k,n} - w_k z_{k,n} + \psi w_k \bar{z}_{k,n}|^2 \right\}$$

where Ω_{CE} is the set of subcarrier symbols used in the estimation.

The idea is to adjust ψ in such a way that difference between the equalizer output and the known pilot $d_{k,n}$ is minimized in the least-squares sense. This is a nonlinear optimization problem, which can be solved using different techniques. We solved this problem by iterating the following two steps:

- 1) Assuming that the phase slope is known from previous iteration (0 in the beginning), $\{w_k^{(i)}\}$ are solved from pilots $z_{k,n} + \psi^{(i-1)} \bar{z}_{k,n}$.
- 2) Assuming that $\{w_k^{(i)}\}$ are known, the observation is linear function of ψ and the optimum $\psi^{(i)}$ can be easily calculated.

This process converges typically in 2-5 iterations.

4.7 Multi-user uplink aspects

In WiMAX, the uplink transmissions are based on FDMA, and different users occupying different subcarriers at the same time are expected to have some differences in their CFO and timing offset values. Then it is necessary to both estimate and compensate the CFOs and timing offsets in frequency domain. The values are kept small enough through feedback of frequency control and timing advance information from base-station to mobiles. Based on the results of Sections 4.5 and 4.6, it is expected that the required CFO and timing offset compensation can be done with very good performance assuming that the residual offsets are within the 802.16e specifications. This will be examined in future studies, together with exploring the possibilities to relax the synchronization specifications and simplifying the related control procedures.

5 Comparison results

In this section, we will assess the performance and compare the different equalizers presented in Section 4 by considering the WiMAX specifications which are recommended in the PHYDYAS project. Here we consider the following WiMAX parameters: $M=1024$, $M_u=840$, $K=4$, $L=KM=4096$, $f_s = 11.2 \text{ MHz}$, 16-QAM modulation and the prototype filter bank suggested by CNAM. We have also considered two types of channels: vehicular A and vehicular B. The former channel has an impulse response shorter than that of the latter one. All the equalizers are also compared to classical OFDM. The CP length for CP-OFDM system is $M/8$. In all simulations, the channel is assumed to be perfectly estimated unless otherwise indicated and only one realization of the used channel is considered.

Figure 5-1 compares multiple band MMSE and simplified MMSE equalizers, MMSE equalizer, equalizers based on frequency sampling method presented in Sections 4.1.1 and 4.1.2, the classical one tap equalizer and CP-OFDM system, in the case of vehicular A channel. Figure 5-1 plots the performance in terms of bit error rate (BER) versus E_b/N_0 . In order to be more objective in comparing the algorithms, we have chosen the same equalizer length, 3, for equalizers MMSE, simplified MMSE, and frequency sampling based equalizers. For the multiple band MMSE equalizer, the equalizer length for the subchannel of interest is 3 and 1 for each adjacent subchannel. We observe that the performance is almost the same for all algorithms. This result can be explained by the fact that with WIMAX specifications given above and vehicular A channel the subchannels are close to be flat and then one tap equalizer is quite enough to equalize the channel. OFDM exhibits similar performance but it should be noted that its throughput rate is smaller than that of the FBMC system, because of the guard interval used in CP-OFDM system. Hence the general performance of FBMC is better.

Figure 5-2 provides the results for a vehicular B channel, which is much more frequency selective. For low SNR all equalizers have roughly the same performance but for high SNR, MMSE and multiple band MMSE outperform the others. We also observe that the CP-OFDM system performance decreases here, due to the insufficient length of the cyclic prefix.

Perfect channel estimates have been used for the above simulations results. Now we investigate the effect of imperfect estimate of the channel. For this purpose, we have considered the channel estimation method presented in Section 3.1. We have also maintained the same simulation parameters given above, with vehicular channel A. For clarity purposes we have considered only the MMSE equalizer, the frequency sampling based equalizer in Section 4.1.2 and CP-OFDM system. Figure 5-3 shows the performance of the equalizers with the actual channel and the estimated one. We observe that, in the case of vehicular A channel and WiMAX parameters, the estimation error does not degrade the performance significantly.

Eventually, for WiMAX parameters, we can say that in the case of short transmission channels, one tap equalizer per subchannel is quite enough because the subchannels are approximately flat. However, for long transmission channels we need subchannel equalizers with more than one tap because subchannels can no longer be approximated as flat. In addition, MMSE seems to be interesting especially in the case of long transmission channels. In terms of complexity, it is clear that the frequency sampling based equalizer in Section 4.1.2 is more attractive than MMSE. We have also seen that multiple band MMSE performs almost like MMSE but with higher complexity. Therefore, it is not of particular interest in our case.

Based on the above discussion, we can conclude that for short transmission channels the classical one tap equalizer represents the best performance/complexity tradeoff. However, for long transmission channels, MMSE is the best. It is worth noting that from a complexity point of view the frequency sampling based equalizer in Section 4.1.2 is more interesting than MMSE.

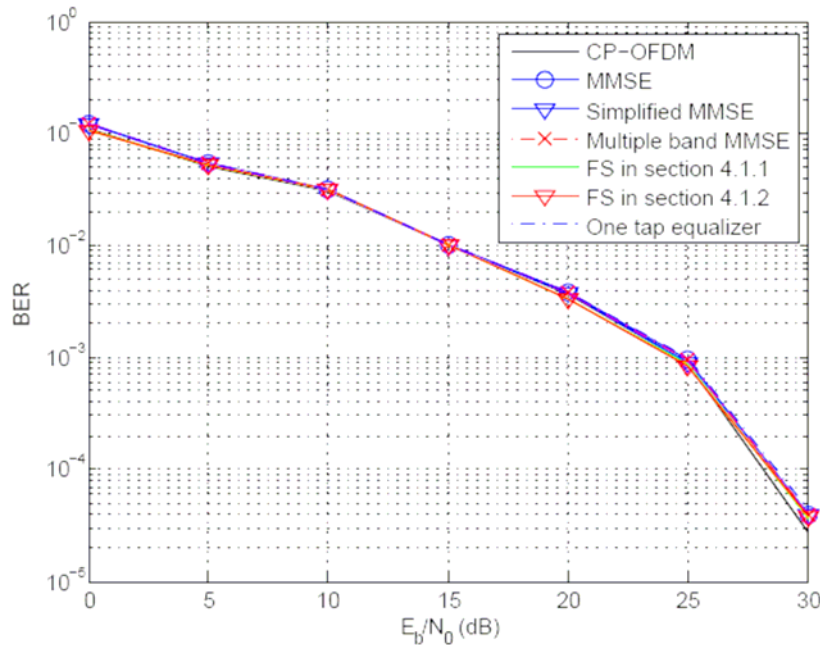


Figure 5-1. Comparison of different equalizers. BER versus E_b/N_0 . $M=1024$ and Veh-A channel.

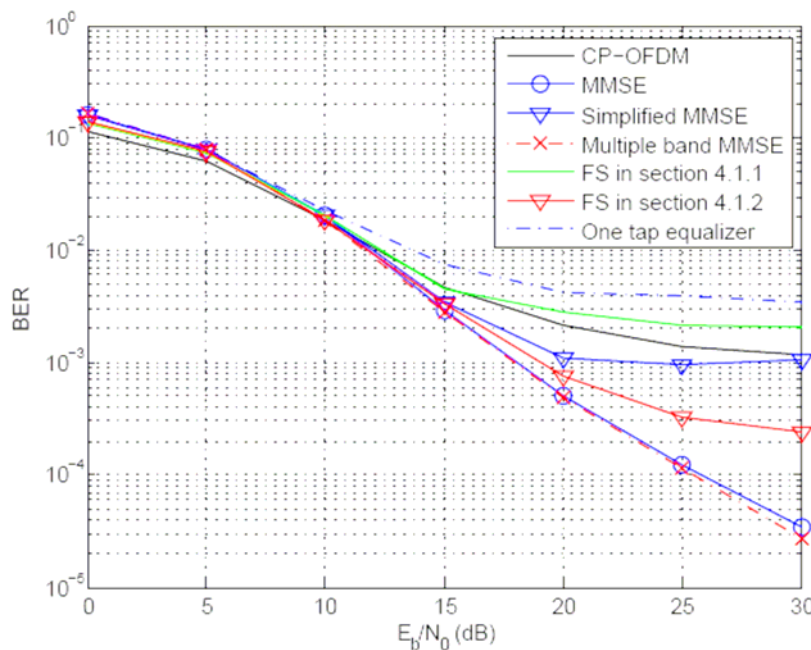


Figure 5-2. Comparison of different equalizers. BER versus E_b/N_0 . $M=1024$ and Veh-B channel.

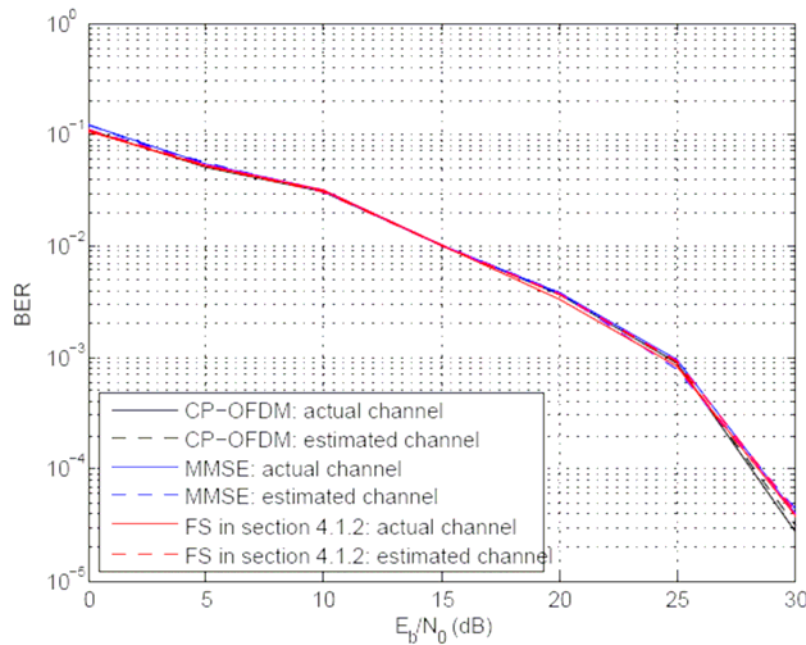


Figure 5-3. Comparison of different equalizers with the actual channel and the estimated one. BER versus E_b/N_0 . $M=1024$ and Veh-A channel.

6 Conclusions and future work

The issue of equalization has been investigated in this document. It has been first focused on channel estimation, which is necessary for the computation of the equalizer. It has been shown that specific pilot configurations can be designed for OQAM systems in order to obtain channel estimates of good quality. The methods also have been adapted to the downlink PUSC mode. However, it still needs to be studied how it can be applied in the uplink PUSC mode.

Several equalizers have then been presented and compared. It appears that in the typical WiMAX environment considered here, a one-tap equalizer is sufficient to obtain good performance. Longer equalizers are however necessary for selective channel, or in order to enhance the correction of the timing error. MMSE and frequency sampling are both interesting techniques to compute equalizers with several taps, depending on the needed performance and the available complexity. In all situations, it has been shown that the performance of FBMC exceeds OFDM. On mildly selective channels, the performance is similar, but FBMC exhibits a higher rate due to the absence of cyclic prefix. On highly selective channels, the performance is even better, despite the higher rate, even though more complex equalizers need to be used.

Finally, the corrections of CFO and timing errors have been discussed. It has been shown that it is possible to compensate for reasonable amount of CFO or timing error in the frequency domain, which is highly desirable in a multi-user environment. The issue of synchronization in the multi-user uplink case still needs to be solved however.

Future work will focus on improving the channel estimation algorithms, on studying bit and power allocation schemes, and on handling synchronization in the multiuser scenario. Further improvement of the OQAM demodulation will also be investigated.

7 References

- [1] P. Siohan, C. Siclet, and N. Lacaille “Analysis and design of OFDM/OQAM systems based on filterbank theory,” *IEEE Trans. Signal Processing*, pp 1170-1183, May 2002.
 - [2] M. G. Bellanger, “Specification and design of a prototype filter for filter bank based multicarrier transmission”, in *Proc. Int. Conf. Acoustics, Speech, and Signal Processing (ICASSP '01)*, pp. 2417 – 2420, May 2001.
 - [3] H. S. Malvar, *Signal Processing with Lapped Transforms*, Artech House, Norwood, Mass, USA, 1992.
 - [4] T. Karp and N. J. Fliege, “Modified DFT Filter Banks with perfect reconstruction,” *IEEE Trans. Circuits and Systems II*, vol. 46, pp. 1404-1414, Nov. 1999.
 - [5] P. P. Vaidyanathan, *Multirate Systems and Filter Banks*, Prentice Hall, Englewood Cliffs, NJ, USA, 1993.
 - [6] T. Ihalainen, T. Hidalgo Stitz, M. Rinne, and M. Renfors, “Channel equalization in filter bank based multicarrier modulation for wireless communications,” *EURASIP Journal on Advances in Signal Processing*, vol. 2007, pp. Article ID 49 389, 18 pages, 2007, doi:10.1155/2007/49389.
 - [7] J.-P. Javaudin, D. Lacroix, and A. Rouxel, “Pilot-aided channel estimation for OFDM/OQAM”, in *Proc. Vehicular Technology Conf. (VTC 2003-Spring)*, pp. 1581-1585, April 2003.
 - [8] C. L   , J.-P. Javaudin, R. Legouable, A. Skrzypczak, and P. Siohan, “Channel estimation methods for preamble-based OFDM/OQAM modulations”, in *Proc. European Wireless (EW'07)*, Paris, France, April 2007.
 - [9] Deliverable 2.1, “Data-aided synchronization and initialization (single antenna),” ICT-211887 PHYDYAS, July 2008.
 - [10] Part 16: Air Interface for Fixed and Mobile Broadband Wireless Access Systems Amendment 2: Physical and Medium Access Control Layers for Combined Fixed and Mobile Operation in Licensed Bands and Corrigendum 1, IEEE Std. 802.16e, 2006.
 - [11] M. Bellanger, “PHYDYAS reference filter bank,” PHYDYAS internal report.
 - [12] M. Bellanger, “Pilot aided channel equalization and measurement – Direct approach,” PHYDYAS internal report.
 - [13] E. Kofidis, D. Katselis, A. Rontogiannis, and S. Theodoridis, “Preamble-based channel estimation methods for OFDM/OQAM systems,” PHYDYAS internal report.
 - [14] D. Lacroix and J.-P. Javaudin, “A new channel estimation method for OFDM/OQAM,” in *Proc. 7th Int'l OFDM Workshop*, Hamburg, Germany, Sept. 2002.
 - [15] C. L   , P. Siohan, R. Legouable, and J.-P. Javaudin, “Preamble-based channel estimation techniques for OFDM/OQAM over the powerline,” in *Proc. ISPLC-2007*, Pisa, Italy, pp. 59–64, March 2007.
-

- [16] C. L    , J.-P. Javaudin, R. Legouable, A. Skrzypczak, and P. Siohan, "Channel estimation methods fo preamble-based OFDM/OQAM modulation", *European Transactions on Telecommunications*, 00:1-16 (2007)-Accepted & Revised. 2008.
 - [17] F. Schaich, "Channel estimation," PHYDYAS internal report.
 - [18] T. Hidalgo Stitz, A. Viholainen T. Ihalainen, and M. Renfors, "Pilot design for PHYDYAS OQAM-FBMC," PHYDYAS internal report.
 - [19] P. H  her, S. Kaiser, and P. Robertson, "Two dimensional pilot symbol aided channel estimation by Wiener filtering," in *Proc. IEEE Int. Conf. on Acoustics, Speech and Signal Processing (ICASSP'97)*, Vol 3, pp. 1845-1848, Munich, Germany. April 21-24, 1997.
 - [20] T. H. Stitz, T. Ihalainen, and M. Renfors, "Practical issues in frequency domain synchronization for filter bank based multicarrier transmission," in *Proc. of Third International Symposium on Communications, Control and Signal Processing*, S. Julians, Malta, March 12-14, 2008.
 - [21] D. S. Waldhauser, L.G. Baltar, and J. A. Nossek, "MMSE subcarrier equalization for filter bank based multicarrier systems," in *Proc. IEEE Workshop on Signal Processing Advances in Wireless Communications (SPAWC'08)*, July 6-9, 2008.
 - [22] J. C. Tu, "Optimum MMSE equalization for staggered modulation," in *Conf. Record of the Twenty-Seventh Asilomar Conf. on Signals, Systems and Computers*, Pacific Grove, CA, Nov. 1-3, 1993, pp. 1401-1406.
 - [23] D. S. Waldhauser, L.G. Baltar, and J. A. Nossek, "Adaptive equalization for filter bank based multicarrier," in *Proc. IEEE Int. Symp Circuits Syst. (ISCAS'08)*, May 18-21, 2008.
 - [24] S. Haykin, *Adaptive Filter Theory*, 4th ed., Prentice Hall, 2001.
 - [25] M. Hawryluck, A. Yongacoglu, and M. Kavehrad, "Efficient equalization of discrete wavelet multi-tone over twisted pair", in *Proc. 1998 International Zurich Seminar on Broadband Communications*, Zurich, Switzerland, Feb. 1998, pp. 185-191.
-